Influences of Morphology and Doping on the Photoactivity of TiO$_2$ Nanostructures

Nasser A. M. Barakat and Muzafar A. Kanjwal

Abstract Compared to the bulk, the nanoscale provides special characteristics for the functional materials. Moreover, the nanostructural morphology has also distinct influences. Enormous efforts have been devoted to the research of TiO$_2$ material, which has led to many promising applications. Beside the morphology impact, doping of titanium dioxide nanostructures by pristine metal nanoparticles (e.g. Ag, Pt, … etc.) revealed distinct improvement in the photocatalytic activity. Although the doping process can remarkably improve the photoactivity, it has also noticeable influences on the crystal structure. In this chapter, the important parameters affecting the photocatalytic activity of TiO$_2$ are discussed; morphology and silver doping. Also, effect of sliver-doping on the crystal structure and the nanofibrous morphology is investigated. Moreover, the influence of the temperature on the photodegradation process using Ag-doped TiO$_2$ nanostructures will be addressed. Two morphologies were introduced; nanoparticles and nanofibers. The nanofibers were synthesized by electrospinning of a sol–gel consisting of titanium isopropoxide, silver nitrate and poly(vinyl acetate). The silver nitrate amount was changed to produce nanofibers having different silver contents. The nanoparticles were prepared from the same sol-gels, however instead of spinning the gels were dried, grinded and sintered. The experimental and analytical studies indicate that doping by silver reveals to form anatase and rutile when the silver nitrate content in the mother solution was more than 3 wt%. The rutile phase content is directly proportional with the AgNO$_3$ concentration. Negative impact of the silver-doping

N. A. M. Barakat (✉)
Organic Materials and Fiber Engineering Department, Chonbuk National University, Jeonju 561-756, Republic of Korea
e-mail: nasser@jbnu.ac.kr

N. A. M. Barakat
Chemical Engineering Department, Minia University, El-Minia 61111, Egypt

M. A. Kanjwal
Technical University of Denmark, DTU Food, Soltofts plads, B 227 2800 Kgs Lyngby, Denmark

on the nanofibrous morphology was observed as increase the silver content caused to decrease the aspect ratio, i.e. producing nanorods rather nanofibers. However, silver-doping leads to modify the surface roughness. In contrast to the known influence of the temperature on the chemical reactions, in case of the nanofibrous morphology of Ag-doped TiO_2, the temperature has negative impact on the photoactivity.

1 Introduction

In chemistry, photocatalysis is the acceleration of a photoreaction in the presence of a catalyst. In catalyzed photolysis, light is absorbed by an adsorbed substrate. In photogenerated catalysis, the photocatalytic activity depends on the ability of the catalyst to create electron–hole pairs, which generate free radicals (e.g. hydroxyl radicals: •OH) able to undergo secondary reactions. Its practical application was made possible by the discovery of water electrolysis by means of titanium dioxide. The commercially used process is called the advanced oxidation process (AOP). There are several ways the AOP can be carried out; these may (but do not necessarily) involve TiO_2 or even the use of UV light. Generally the defining factor is the production and use of the hydroxyl radical. Generally, the semiconductors are used as photocatalysts. Like other solids, semiconductor materials have electronic band structure determined by the crystal properties of the material. The actual energy distribution among the electrons is described by the Fermi energy and the temperature of the electrons. At absolute zero temperature, all of the electrons have energy below the Fermi energy; but at non-zero temperatures the energy levels are filled following a Boltzmann distribution.

In semiconductors the Fermi energy lies in the middle of a forbidden band or band gap between two allowed bands called the valence band and the conduction band. The valence band, immediately below the forbidden band, is normally very nearly completely occupied. The conduction band, above the Fermi level, is normally nearly completely empty. Because the valence band is so nearly full, its electrons are not mobile, and cannot flow as electrical current.

However, if an electron in the valence band acquires enough energy to reach the conduction band, it can flow freely among the nearly empty conduction band energy states. Furthermore it will also leave behind an electron hole that can flow as current exactly like a physical charged particle. Carrier generation describes processes by which electrons gain energy and move from the valence band to the conduction band, producing two mobile carriers; while recombination describes processes by which a conduction band electron loses energy and re-occupies the energy state of an electron hole in the valence band.

In a material at thermal equilibrium generation and recombination are balanced, so that the net charge carrier density remains constant. The equilibrium carrier density that results from the balance of these interactions is predicted by

thermodynamics. The resulting probability of occupation of energy states in each energy band is given by Fermi–Dirac statistics.

Fast electrons/holes recombination is the main dilemma facing the semiconductors photocatalysts in general and titanium oxide in particular. Incorporation of noble metal nanoparticles (NPs) into the titania dielectric matrix is a recent strategy to overcome this problem and simultaneously improve the photocatalytic activity of titanium oxide [1, 2]. Doping with foreign metal nanoparticles can produce high Schottky barrier that facilitates electron capture [3]. The capture of electrons postulate to produce a longer electron–hole pair separation lifetime, and therefore hinder the recombination of electron/hole pairs and enhance the transfer of holes and possibly electrons to O_2 adsorbed on the TiO_2 surface. Afterwards, excited electrons migrate to the metal, where they become trapped and the electron/hole pair recombination is suppressed. Therefore, many investigations have reported the enhancement of photoactivities in both liquid and gas phases [4, 5]. Moreover, this incorporation provides an absorption feature due to the surface plasmon resonance (SPR) occurring over the visible range of the spectrum [6]. Particularly, silver and gold nanoparticles are more familiar because of their color varieties in the visible region, which is attributed to oscillations of the electrons at the surface of the nanoparticles [7]. Silver is the most common metal used to modify titania, because its *d-s* band gap is in the UV region and does not damp out the plasmon mode as strongly as gold [8, 9]. Titania-modified-silver particles have raised extensive interest due to their applications in photocatalytic degradation [10]. The researchers have intensively studied how silver provides titania distinct photocatalytic activity, the mechanism has been well explained in previous reports [11–13]. Moreover, some researchers have concluded that incorporation of silver in titanium dioxide leads to increases in the total surface area of the prepared titanium dioxide [14, 15]. This can be considered an additional benefit of utilizing silver-loaded titanium oxide in the field of photocatalytic degradation. Therefore, many researchers have practically demonstrated that the degradation rates of the dyes can be enhanced by the deposition of silver on titanium dioxide [16–18].

In the last decades, nanostructural materials have been intensively investigated because of their high surface area, which strongly affects their physiochemical properties. Different shapes have been introduced. Of the reported nanostructure shapes, special attention has been paid to one-dimensional forms such as nanorods, nanowires, and nanofibers. This is due to their potential applications in the nanodevices [19–21]. Nanofibers have received special consideration due to their high axial ratio, good mechanical properties, and their manageable and novel physical properties.

Compared to nanoparticles, nanofibers have small surface area which might be considered a negative impact upon using as catalyst in the chemical reactions. Therefore, if the morphology has no impact, the nanoparticles will have higher catalytic activity. Moreover, for the same surface activity, the temperature should have the same influence on both formulations. In most of the chemical reactions, positive effect of the temperature on the reaction rates is a prevailing impression. Temperature is a measure of the kinetic energy of a system, so higher temperature

implies higher average kinetic energy of molecules and more collisions per unit time. This hypothesis might be true in the normal cases, however the nanostructures usually have unexpected behaviors compared to the bulk scales.

In this chapter, the aforementioned facts have been investigated for the Ag-doped TiO_2 nanophotocatalyst. Two nano-formulations have been utilized; nanofibers and nanoparticles. Silver-grafted titanium oxide nanofibers have been synthesized using the electrospinning of silver nitrate/titanium isopropoxide/poly(vinyl acetate) sol–gel. However, the nanoparticulate form has been obtained by calcination of a ground powder prepared from the same electrospun sol–gels. Metal-doping may also have an influence on the titania crystal structure leading to distinct improving in the application fields [22, 23]. Therefore, effect of the silver-doping on the crystal structure, the morphology and the photocatalytic activity of TiO_2 nanofibers will be discussed in this chapter.
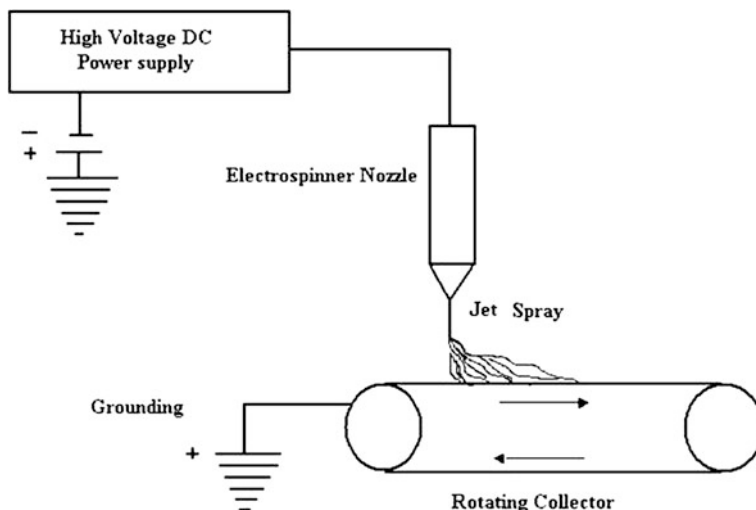
2 Nanofibers

Nanofibers are an exciting new class of material used for several value added applications such as medical, filtration, barrier, wipes, personal care, composite, garments, insulation, and energy storage. Special properties of nanofibers make them suitable for a wide range of applications from medical to consumer products and industrial to high-tech applications for aerospace, capacitors, transistors, drug delivery systems, battery separators, energy storage, fuel cells, and information technology [24, 25].

If the diameters of polymer fiber materials are shrunk from micrometers to submicrons or down to nanometers, there appear several amazing characteristics such as very large surface area to volume ratio (this ratio for a nanofiber can be as large as 10^3 times of that of a microfiber), flexibility in surface functionalities, and superior mechanical performance (e.g. stiffness and tensile strength) compared with any other known form of the material. These outstanding properties make the polymer nanofibers to be optimal candidates for many important applications [26].

Generally, polymeric nanofibers are produced by an electrospinning process (Fig. 1). Electrospinning is a process that spins fibers of diameters ranging from 10 nm to several hundred nanometers. This method has been known since 1934 when the first patent on electrospinning was filed. Fiber properties depend on field uniformity, polymer viscosity, electric field strength and DCD (distance between nozzle and collector). Advancements in microscopy such as scanning electron microscopy has enabled us to better understand the structure and morphology of nanofibers. At present the production rate of this process is low and measured in grams per hour.

Another technique for producing nanofibers is spinning bi-component fibers such as Islands-In-The-Sea fibers in 1–3 denier filaments with from 240 to possibly

Fig. 1 Schematic representation of electrospinning process

as much as 1,120 filaments surrounded by dissolvable polymer. Dissolving the polymer leaves the matrix of nanofibers, which can be further separated by stretching or mechanical agitation.

The most often used fibers in this technique are nylon, polystyrene, polyacry-lonitrile, polycarbonate, PEO, PET and water-soluble polymers. The polymer ratio is generally 80 % islands and 20 % sea. The resulting nanofibers after dissolving the sea polymer component have a diameter of approximately 300 nm. Compared to electrospinning, nanofibers produced with this technique will have a very narrow diameter range but are coarser.

In the electrospinning process, the solution is held at the tip of a capillary tube by virtue of its surface tension. The electrical potential applied provides a charge to the polymer solution. Mutual charge repulsion in the polymer solution induces a force that is directly opposite to the surface tension of the polymer solution. An increase in the electrical potential initially leads to the elongation of the hemispherical surface of the solution at the tip of the capillary tube to form a conical shape known as the Taylor cone [27]. A further increase causes the electric potential to reach a critical value, at which it overcomes the surface tension forces to cause the formation of a jet that is ejected from the tip of the Taylor cone. The charged jet undergoes bending instabilities and gradually thins up in air primarily due to elongation and solvent evaporation [28]. The charged jet eventually forms randomly oriented nanofibers that can be collected on a stationary or rotating grounded metallic collector of the electrospinning set up [29].

2.1 Metallic Nanofibers

In recent years, ceramic material with effective control at the nanometer scale has been actively pursued as a problem of materials science and engineering. In particular, the preparation of 1D ceramic nanostructures such as fibers, wires, rods, belts, tubes, spirals, and rings has received great interest owing to their potential applications in many vital areas of technologically such as electronics, photonics, and mechanics [30, 31]. A large number of chemical and/or physical methods, mostly based on the bottom-up and template directed routes, have been demonstrated for producing 1D ceramic nanostructures with various compositions by controlling the nucleation and growth processes. Top-down approaches such as photolithography, soft lithography and electrospinning have also been exploited to fabricate 1D ceramic nanostructures [30, 32–35]. Moreover, electrospinning of vital materials are fascinating in the field of implantology. Electrospinning of metallic nanofibers has been largely limited due to availability of proper solvent and desired viscosity for bending instability during electrospinning process. Ceramics are usually considered to be not directly spinnable although it is possible (at least, in principle) to electrospun ceramic nanofibers from their melts at extremely high temperatures. Like conventional spinning processes for generating ceramic fibers. Preparation of ceramic fibers by electrospinning has to rely on the use of spinnable precursors or by using a blending template containing colloidal sol [36]. The fabrication of ceramic nanofibers consists of three major steps:

- Preparation of an inorganic sol or a solution containing a matrix polymer together with an alkoxide, salt, or polymer precursor.
- Electrospinning of the solution to generate composite nanofibers consisting of the matrix polymer and precursor. The spinning experiments are usually performed in a well-controlled environment at room temperature.
- Calcination, sintering, or chemical conversion of the precursor into the desired ceramic at an elevated temperature, with concomitant removal of all organic components from the precursor fibers.

As compared with the bulk metals, these nanofibers have been approved to be an excellent templates for the bottom based applications. This potentiality is the basis for superior properties like less weight, high area to volume ratio, improved durability and bioactive interfaces [37–41].

2.2 Modification of Titania Nanofibers

Currently, the heterogeneous photocatalysis has arised as an alternative economical and harmless technology for removal of organic impurities. In such processes, the illuminated semiconductors absorb light and generate electronic species which

leads to complete oxidation of organic components in waste waters. Titanium dioxide is considered an interesting material because of its optical, electrical and photochemical properties [42, 43]. However, for practical applications the photocatalytic activity and photoresponse behavior of titanium dioxide are very much needed to be further improved [5, 44]. Recently studies have focussed to modify the surface of titanium dioxide to improve its efficiency for photocatalytic activity and to use in solar cells [5, 45]. Incorporation of noble metal nanoparticles into the titania dielectric matrix is a modern strategy to improve the photocatalytic character of titanium dioxide. This incorporation is providing an absorption feature due to surface plasmon resonance (SPR) occurring over the visible range of the spectrum [6]. In particular, silver and gold metals are the most popular materials do have strong SPR character [46, 47]. Moreover, the nanoscale noble metals are usually classical high-performance heterogeneous catalysts [43, 48]. Silver is the most common metal used to modify titania that is because of its *d-s* band gap is in the UV region and does not damp out the plasmon mode as strongly as for gold [8, 9]. The titania modified-silver particles have raised an extensive interest due to their applications in photocatalytic degradation [10]. The researchers have intensively studied how silver provides titania distinct photocatalytic activity; the mechanism was well explained [11–13, 49–52]. Many formulations have been introduced for titania/silver composite, for instance, nanoparticles [53], and thin films [54–56].

As it is well known, the surface to volume ratio is an important feature for any catalyst. Accordingly, 1D nanostructures are expected to strongly modify the photocatalytic activity. Among all 1D nanostructure, nanofibers do have especial interest due to large surface area to volume ratio. In the field of metal oxides nanofibers; electrospinning is the most widespread.

3 Experimental Section

3.1 Materials

Silver nitrate (99.8 assay), methylene blue dihydrate dye (95.0 assay), N,N-dimethylformamide (DMF, 99.5 assay), and rhodamine B dye were obtained from Showa, Co. Japan. Titanium (1V) isopropoxide (Ti(Iso), 98.0 assay) was purchased from Junsei Co. Ltd., Japan. Poly (vinyl acetate) (PVAc, MW = 500,000 g/mol) was obtained from Aldrich, USA. These materials were used without any further purification.

3.2 Preparation of Nanofibers and Nanoparticles of Ag/TiO$_2$ Composite

3.2.1 Nanofibers

The electrospinning process was utilized to prepare the silver-grafted titania Nanofibers (NFs). Typically, a sol–gel was prepared by mixing titanium iso-propoxide (Ti(Iso)) and poly(vinyl acetate) (PVAc, 14 wt% in DMF) with a weight ratio of 2:3, respectively, and then few drops of acetic acid were added until the solution became transparent. The mixing process was carried out at 25 °C using magnetic stirrer rotating at 150 rpm. To prepare sol–gels containing different contents of silver, silver nitrate solutions in DMF were mixed with proper quantities of the prepared Ti(Iso)/PVAc solution to prepare final solutions containing 0.5, 1.0, 1.5, 2.0 and 2.5 wt% AgNO$_3$. Afterwards, these solutions were homogeneously mixed under stirring conditions for 10 min at 25 °C and moderate stirring speed. A high voltage power supply (CPS-60 K02V1, Chungpa EMT Co., Republic of Korea) was used as the source of the electric field. The sol–gel was supplied through a plastic syringe attached to a capillary tip. A copper wire originating from the positive electrode (anode) connected with a graphite pin was inserted into the sol–gel and the negative electrode (cathode) was attached to a metallic collector covered with polyethylene sheet. Briefly, the solution was electrospun at 6 kV and 15 cm working distance (the distance between the needle tip and the collector). The electrospinning process was carried out at 25 °C in 40 % relative humidity atmosphere. The formed nanofiber mats were initially dried for 24 h at 80 °C in a vacuum and then calcined in air atmosphere at 700 °C for one hour with a heating rate of 5 °C/min.

3.2.2 Nanoparticles

Silver nitrate/Ti(Iso)/PVAc solutions having the aforementioned compositions and preparation procedure were utilized to prepare nanoparticles containing different silver contents. The process parameters (temperature and stirring) were not changed. Instead of spinning, the solution was vacuously dried at 80 °C for 48 h to completely remove the solvent. The obtained solid materials were finely grinded and sintered in air at 700 °C for 1 h.

3.3 Photocatalytic Degradation

The photocatalytic degradation of the selected dyes in the presence of Ag-TiO$_2$ nanofibers and nanoparticles was carried out in a simple photo reactor. The reactor was made of glass (1,000 ml capacity, 23 cm height and 15 cm diameter), covered

with aluminum foil, and equipped with ultra-violet lamp emitting radiations at 365 nm. The initial dye solution and the photocatalyst were placed in the reactor and continuously stirred to ensure proper mixing during the photocatalytic reaction. Typically, 100 ml of dye solution (10 ppm, concentration) and 50 mg of catalyst were used. At specific time intervals, a 2 ml sample was withdrawn from the reactor and centrifuged to separate the residual catalyst, and then the absorbance intensity was measured at 664 and 554 nm for methylene blue and rhodamine B dyes, respectively.

3.4 Characterization

Surface morphology of nanofibers was studied by JEOL JSM-5900 scanning electron microscope (JEOL Ltd, Japan) and field-emission scanning electron microscope (FESEM, Hitachi S-7400, Japan). The phase and crystallinity were characterized by using Rigaku X-ray diffractometer (Rigaku Co, Japan) with Cu Kα ($\lambda = 1.54056$ Å) radiation over a range of 2θ angles from 20° to 100°. High resolution image and selected area electron diffraction pattern were observed by JEOL JEM-2200FS transmission electron microscope (TEM) (JEOL Ltd., Japan). The concentration of the dyes during the photodegradation study was investigated by spectroscopic analysis using HP 8453 UV–visible spectroscopy system (Germany). The spectra obtained were analyzed by HP ChemiStation software 5890 series.

4 Results and Discussion

4.1 The Photocatalyst Characterization

The polymer is an essential constituent in sol–gels to achieve the electrospinning process [19, 57–59]. Metal alkoxides are the best candidates to form the gel structure due to their affinity to hydrolysis and condensation in the polymer matrix. Because of the well polycondansation property [60, 61], titanium isopropoxide is a famous precursor to prepare TiO_2 nanofibers by using the electrospinning process and PVAc as a gelling polymer [62]. Addition of silver nitrate does not affect the nanofibrous morphology [5]. Figure 2a displays the obtained PVAc/Ti(Iso)/ $AgNO_3$ (the later was 2.0 wt% in the electrospun solution) nanofibers. As shown, good morphology was obtained. It is noteworthy mentioning that all the formulations produced good morphology nanofibers; only slight decrease in the average fiber diameter with increasing the silver nitrate content was observed due to increase the electrical conductivity of the electrospun solutions. Calcination did not affect the nanofibrous morphology for all formulations. Figure 2b represents

the SEM image of the obtained powder from calcination of the electrospun mat containing 2.0 wt% silver nitrate. As shown, good nanofibers were obtained. Increase the roughness of the outer surface with increasing the silver nitrate content in the original electrospun sol–gel was a noticeable observation. Figure 2c and d display the FE SEM images of the pristine and Ag-containing ($AgNO_3$ = 2.0 wt%) TiO_2 nanofibers, respectively. Big difference between the surfaces of the investigated nanofibers can be observed. It is noteworthy mentioning that the surface roughness was dependent on the silver content, moreover increase the silver nitrate content more than the maximum value used in this study (i.e. 2.5 wt%) led to destroy the nanofibrous morphology and produce nanorods instead. Concerning the nanoparticulate shape, addition of silver nitrate improves the spherical morphology of the nanoparticles as shown in Fig. 2e and f which demonstrate the SEM images of the pristine and Ag-doped (2.0 wt%) TiO_2 nanoparticles.

To properly investigate the effect of addition of silver nitrate on the surface of the silver-doped nanofibers, the surface area has been measured by using Brunauer–Emmett–Teller (BET) technique (Micromeritics, Norcross, GA). The obtained results indicated that the average surface area of the silver-free nanofibers was about 21.3102 ± 0.1351 m^2/g, while, it was 38.8100 ± 0.1324 m^2/g for the nanofibers obtained from calcination of silver nitrate (2 wt%)/Ti(Iso)/PVAc electrospun nanofiber mats. As can be concluded from these results, the surface area of the silver containing nanofibers was duplicated compared to the pristine ones which strongly enhance the photocatalytic activity. For the nanoparticles, it is clear from the SEM images that addition of silver has negative influence on the surface area as the average diameter decreases with silver addition (Fig. 2e and f).

XRD is a reliable and widespread identification technique especially for crystalline materials. Figure 3 represents the XRD pattern of the nanofibers obtained from two sol–gels, Ti(Iso)/PVAc and silver nitrate (2.0 wt%)/Ti(Iso)/PVAc. As shown in both spectra, the results confirm formation of pure anatase titanium dioxide. The strong diffraction peaks at 2θ values of 25.09°, 37.65°, 38.44°, 47.89°, 53.89°, 55.07°, 62.40°, 68.70°, 70.04°, and 75.00° correspond to the crystal planes (101), (004), (112), (200), (105), (211), (204), (220), (220), and (215), respectively indicate formation of anatase titanium dioxide [JCPDS card no 21-1272]. In the case of the nanofibers obtained from calcination of silver nitrate/Ti(Iso)/PVAc mats (Fig. 2, spectra A), in addition to the titanium dioxide peaks, extra peaks at 2θ values of 38.11°, 44.29°, 64.43° and 77.48° corresponding to the crystal planes (111), (200), (220), and (311), respectively confirm presence of silver metal [JCPDS card no 04-0783]. To make it easy, in Fig. 3, we have marked the peaks corresponding to titanium oxide and silver as A and S, respectively. It is noteworthy to mention that the morphology did not affect the XRD data (i.e. the same results have been obtained for the nanoparticles). Therefore, the XRD pattern of the nanoparticles was not added to simplify and clarify the figure.

Transmission electron microscope analysis is used to investigate the crystal structure. Figure 3 shows the HR TEM of the obtained Ag-doped TiO_2 nanofibers; A and nanoparticles; B. As shown in these figures, there are some black dots in
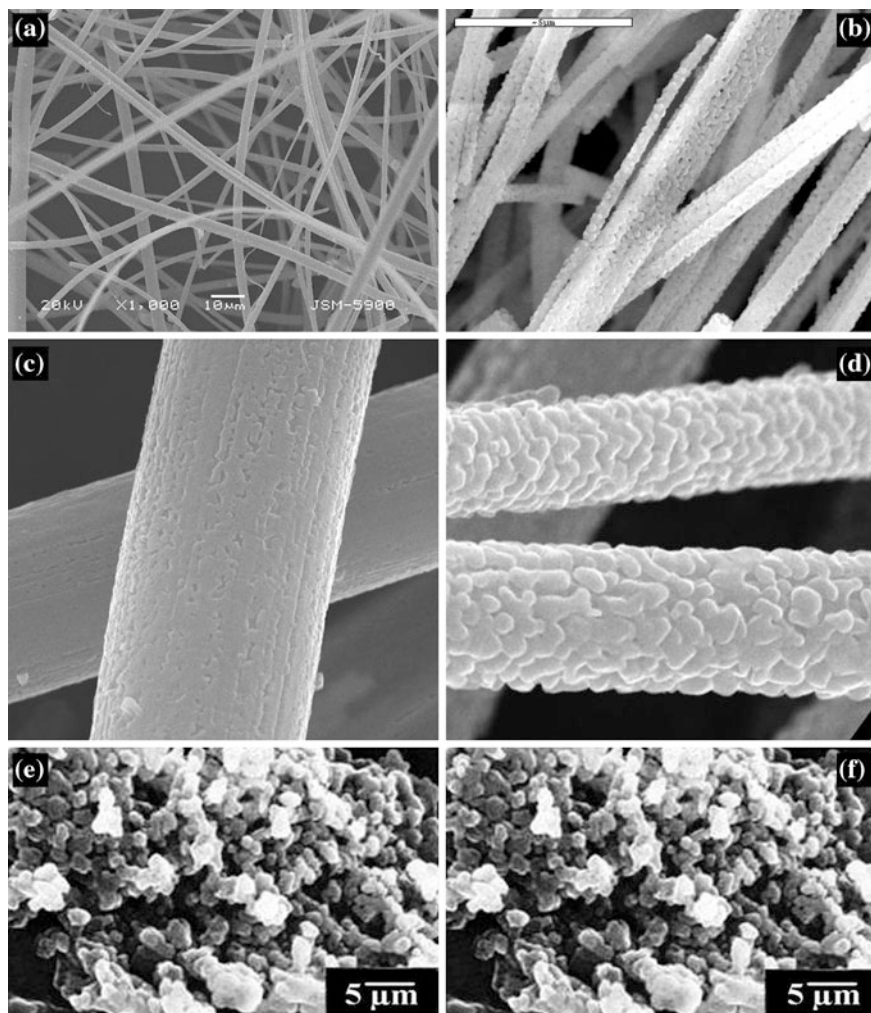
**Fig. 2** SEM image of the electrospun PVAc/Ti(Iso)/AgNO$_3$ (AgNO$_3$ = 0.2) nanofibers; **a** the corresponding sintered nanofibers; **b** FE SEM images of the pristine; **c** and Ag-doped TiO2; **d** nanofibers, and SEM images of the pristine; **e** and Ag-doped TiO$_2$ (AgNO$_3$ = 0.2); **f** nanoparticles

both formulations which can be considered as the Ag nanoparticles as these dots have different crystal structures compared to the TiO$_2$ matrices. Both formulations have good crystallinity as shown in Fig. 4c and d which represent the SAED patterns of the Ag-doped TiO$_2$ nanofibers and nanoparticles, respectively. Moreover, the Fast Fourier Transform (FFT) images for both formulations reveal good crystallinity as shown in the corresponding insets.
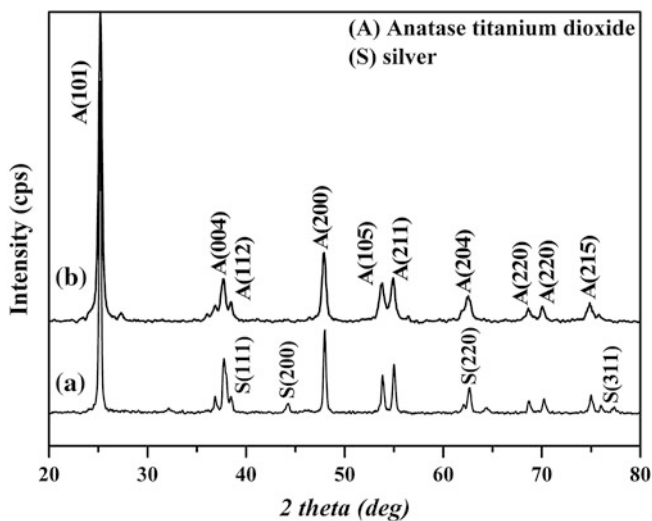
Fig. 3 XRD results for the obtained powder after calcination of PVAc/Ti(Iso) and PVAc/Ti(Iso)/AgNO$_3$ (AgNO$_3$ = 0.2) electrospun nanofibers in air at 700 °C
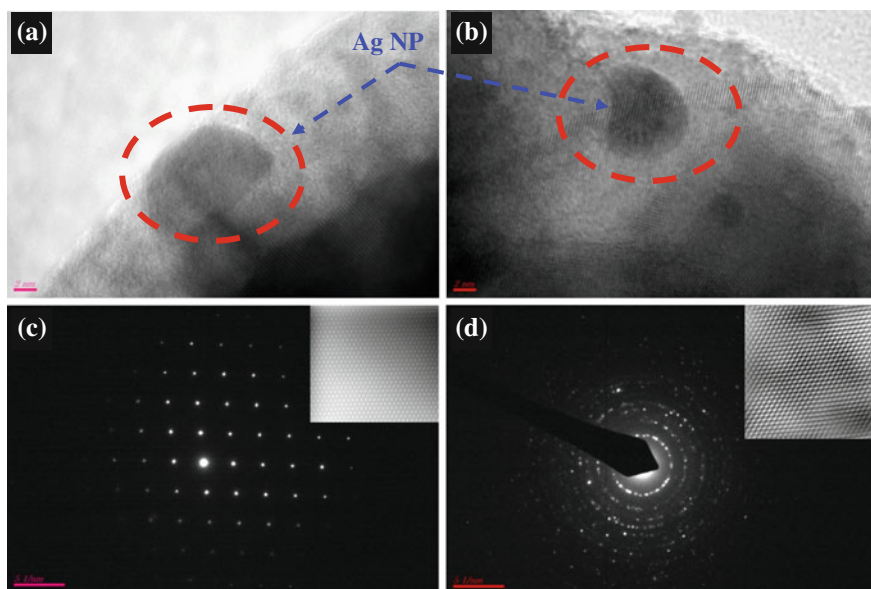
Fig. 4 HR-TEM image of the Ag-doped TiO$_2$ nanofibers; **a** and nanoparticles; **b** and SAED patterns of the marked areas; **c** and **d** the insets show the FFT images of the marked areas

In order to affirm that the silver is present as particles in the TiO_2 nanofibers and simultaneously investigate the nanoparticles appeared in the TEM images, EDX analysis has been invoked. The analysis has been performed in two different points as shown in Fig. 5. As shown in this figure and the corresponding insets, there is big difference in the silver weight percentages between the two chosen points. Therefore, one can say that the point in Fig. 5a represents a point containing silver nanoparticles since the silver content at that point is almost 21 %. However, Fig. 5b might represent almost silver-free point. Taking into consideration that the electron beam in the EDX analysis has specific width more than the silver nanoparticle size, the small weight percentage of silver at this point might be explained as a small part of bordering silver nanoparticles. Actually, these results match all the previous reports about silver-doped titania nanostructures which concluded that the silver exists as small nanoparticles in/on the synthesized nanostructures. Moreover, according to the atomic size, silver-titania system cannot form solid solution alloy, so, theoretically silver has to be in the form of nanoparticles within the titania matrix. Well distribution of silver nanoparticles can be obtained by good mixing of the original $AgNo_3$-Ti(Iso)-PVAc mixture, so, in this study, the electrospinning process was achieved after obtaining well mixed solution.

To explain the phase changes during the calcination process of both formulations (i.e. Ti(Iso)/PVAc and silver nitrate-Ti(Iso)/PVAc), we have utilized thermal gravimetric analysis (TGA). Figure 6 shows the obtained TGA results in all cases,
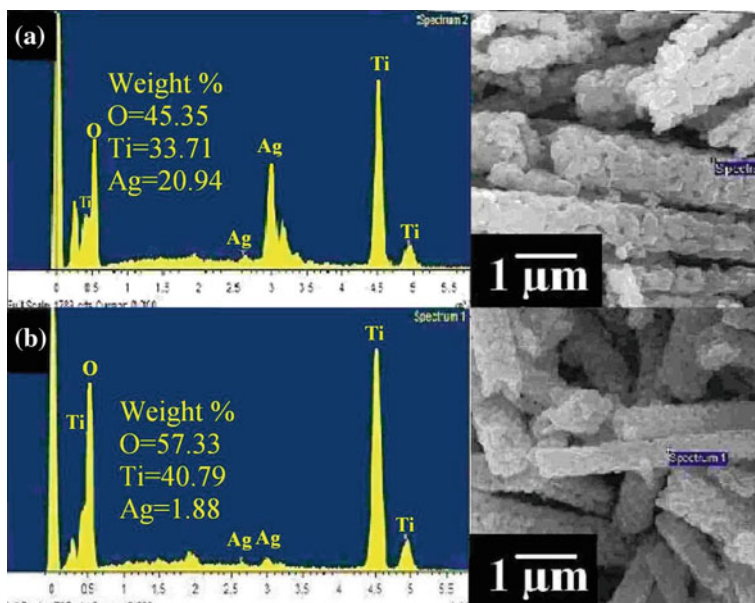
Fig. 5 EDX analysis at two different points, the insets represent the corresponding elemental weight percentages

along with the first derivatives curves were plotted to precisely extract the useful information. Figure 6a represents TGA results for Ti(Iso)/PVAc nanofiber mats, as shown in this figure; two peaks are observed in the first derivative plot. According to the thermal properties of titanium isopropoxide, the first peak (at ~325 °C) can be explained as decomposition of this organometallic compound into titanium
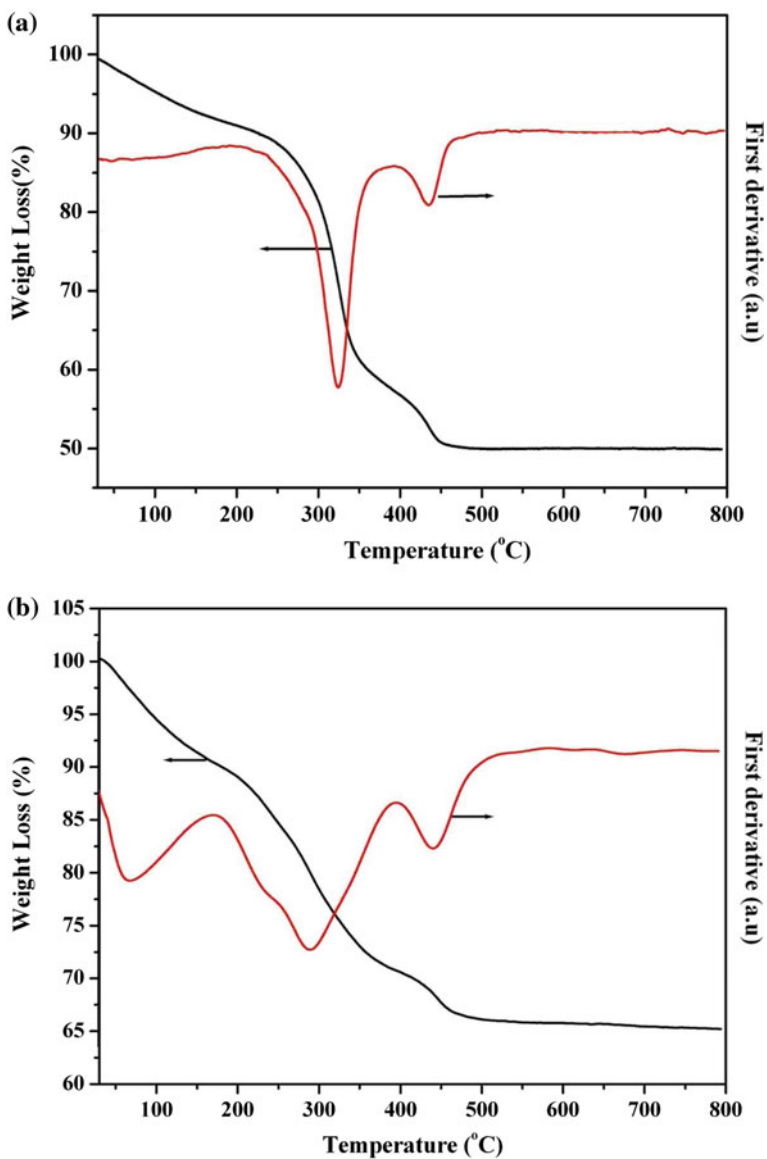
Fig. 6 TGA results in oxygen atmosphere for Ti(Iso)/PVAc (**a**) and silver nitrate-Ti(Iso)/PVAc nanofiber mats (**b**)

dioxide. Because of the calcination process has been performed in air atmosphere, the second peak (at ∼434 °C) can be explained as complete elimination of PVAc that also matches our previous work in the same polymer [5]. However, in case of silver nitrate- Ti(Iso)/PVAc (Fig. 6b), there are observable change; as shown in this figure, the rate of degradation is comparatively low compared with the first case. Also, there are two main peaks were obtained, a broad peak at ∼286 °C and another one at 445 °C. According to the thermal properties of silver nitrate [59], and Ti(Iso) (as seen in Fig. 6a), the first peak can be investigated as simultaneous decomposition of silver nitrate and Ti(Iso). However, the second peak represents the decomposition of PVAc polymer. There is another peak at low temperature (∼60 °C) it might be explained as evaporation of the combined moisture with the sample. Another observation can be noticed by comprising the thermal decomposition of the two formulations is increase the final inorganic residuals in case of the silver nitrate-Ti(Iso)/PVAc than the silver-free case, this increase represents the silver NPs.

4.2 Effect of Silver Doping on the Photoactivity of the Titania

To investigate the influence of the silver doping on the photoactivity of titanium oxide, photodegradation of some organic dyes was performed as explained in the experimental section.

4.2.1 Methylene Blue Dihydrate dye

To safely estimate the dye concentration in the distilled water, the absorbance intensities of the utilized methylene dye have been measured for many dye/distilled water solutions. The UV absorbance spectra for different concentrations of dye solutions (starting from 1 to 8.75 mg/l) were measured within the range of 500–800 nm. Figure 7a reveals the obtained results. As shown in this figure, the absorbance curves have maximum value at almost 664 nm. Moreover, the maximum measured absorbance intensities were linearly increased with increasing of the dye concentration as shown in Fig. 7b which represents the relationship between the dye concentration and the measured absorbance at 664 nm. As shown in this figure, the absorbance varies linearly with the dye concentration in good model. Statistical analyses of this curve indicated high accuracy of the exploited linear model since the coefficient of determination; R^2 of this model was 0.9989 which reveals excellent precision and reproducibility of this calibration curve.

Theoretically, as mentioned in the introduction section some studies have explained the role of silver in enhancing the photocatalytic activity of titania. Generally, these studies have drawn this conclusion. The Ag nanoparticles
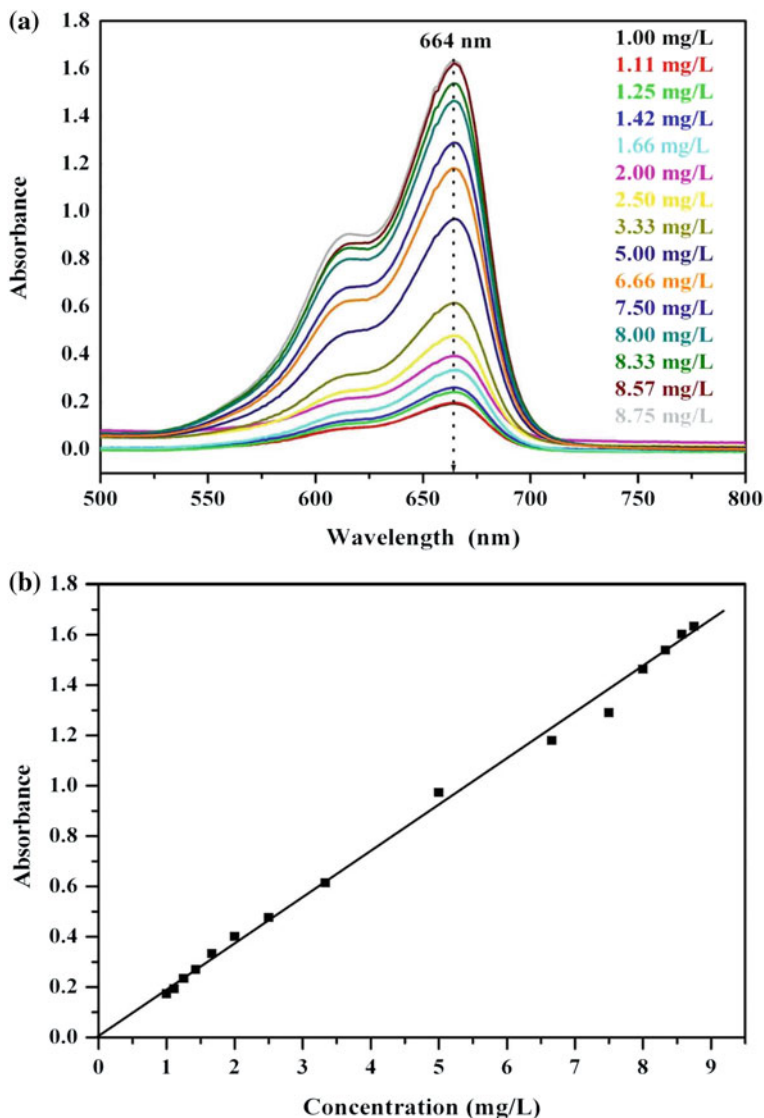
Fig. 7 Absorbance spectra at different concentrations of methylene blue dye solutions within a range of 500–800 nm (**a**), and the relationship between the absorbance intensity and concentration of the dye at wavelength of 664 nm (**b**)

deposited on TiO_2 surface act as electron acceptors, enhancing the charge separation of electrons and holes and consequently the transfer of the trapped electron to the adsorbed O_2 acting as an electron acceptor. The sufficient dye molecules are adsorbed on the surface of Ag-TiO_2 than on the TiO_2 surface, increasing the

photoexcited electron transfer from the sensitised dye molecule to the conduction band of TiO_2 and consequently increasing the electron transfer to the adsorbed O_2.

Experimentally, the pure titania and silver-doped titania nanofibers have been invoked as photocatalysts in degradation of methylene blue dye, Fig. 8 shows the obtained results. As shown in this figure, incorporating of silver in titanium oxide nanofibers reveals to significant increase in the degradation rate of this dye. As can be observed in this figure, within 10 min more than 92 % of the dye has been degraded, moreover, the dye completely eliminated after almost two hours. This interesting result comes from exploiting the advantage of the nanofibrous shape as well as the benefit of incorporating of silver in titanium oxide. However, in case of pure titanium oxide nanofibers, almost 50 % of the dye has been oxidized after 30 min and the dye was almost disappeared from the solution after 6 h. Actually, even in case of pure titanium nanofibers, the obtained results are satisfactory compared with the other photocatalyst [63].
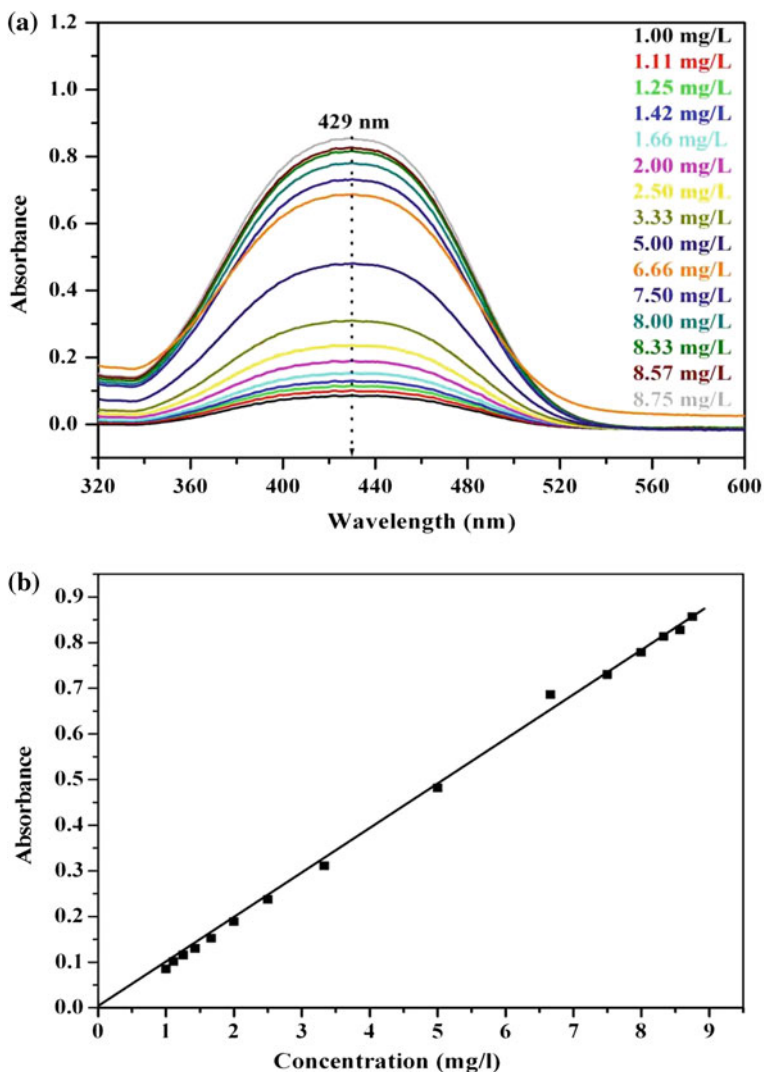
4.2.2 Methyl Red Dye

By the same aforementioned fashion, the wavelength corresponding to maximum absorbance intensity in case of methyl red dye has been estimated. Figure 9a shows the relationships between the absorbance intensity and the wavelength for many dye aqueous solutions (from 1 to 8.75 ppm) within wavelength range of 300–600 nm. As shown in the figure, the wavelength matching maximum
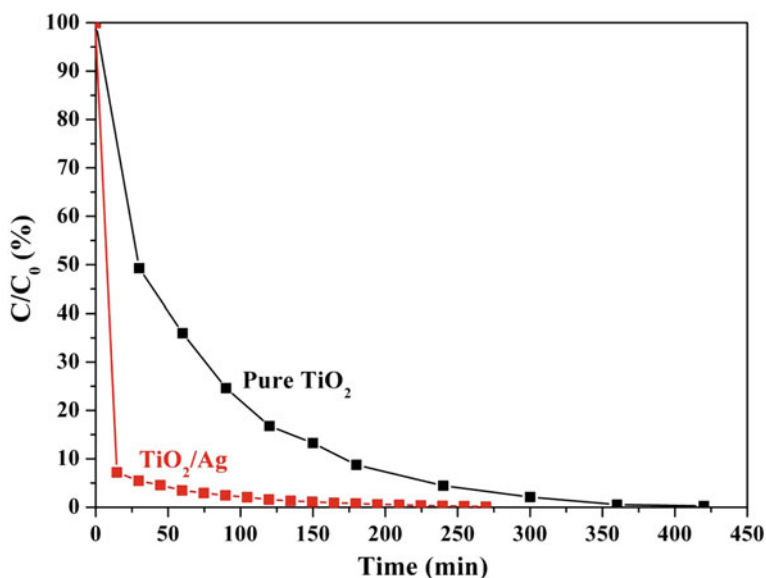
Fig. 8 Photocatalytic degradation of methylene blue dye in presence of pure TiO_2 and Ag-TiO_2 nanofibers

absorbance intensity for all dye concentrations is 428 nm. Moreover, there is very good linearity between the dye concentration and the absorbance intensity at this wavelength as shown in Fig. 9b. A single calibration model was adequate to represent all the data points in Fig. 9b with very low mathematical errors ($R^2 = 0.999$). Therefore, one can confidently apply in this calibration curve (Fig. 9b) to estimate the concentration of any unknown methyl red dye aqueous solution after measuring the absorbance intensity for this solution at 428 nm.

Fig. 9 Absorbance spectra at different concentrations of methyl red dye solutions within a range of 300–600 nm (**a**), and the relationship between the absorbance intensity and concentration of the dye at wavelength of 428 nm (**b**)

It is worth noting that methyl red decay is only due to photocatalysis as already published results showed practically no dye removal by only UV radiation within 300 min [42]. Accordingly, it is difficult to completely remove this dye within relatively short reaction time; e.g. several hours [42]. Figure 10 reveals the obtained results after utilizing the prepared TiO_2 and Ag/TiO_2 nanofibers as photocatalysts to oxidize the methyl red dye. As shown in this figure, the behavior of this dye is completely different than methylene blue, in contrast to that dye; the same removal percentage (i.e. 92 %) was obtained after almost 3 h. Actually, this result is also very satisfactory since according to our best knowledge, no one has reached to such decay percentage using any photocatalyst. Moreover, this result affirms the role of silver in enhancement of the behavior of titanium oxide as photocatalyst since the nanofibrous shape was not enough to eliminate this dye as shown in Fig. 10. Almost 50 % of the dye is remaining after 7 h, this decay efficiency is not rejected compared with the other catalysts [64].

4.3 Effect of Morphology

The effect of the fibrous morphology has been investigated by studying the rates of degradation of methylene blue dye using the two formulations as photocatalyst. The obtained results have strongly recommended utilizing this composite in nanofibrous form. Figure 11 represents the effect of nanostructure shape on the
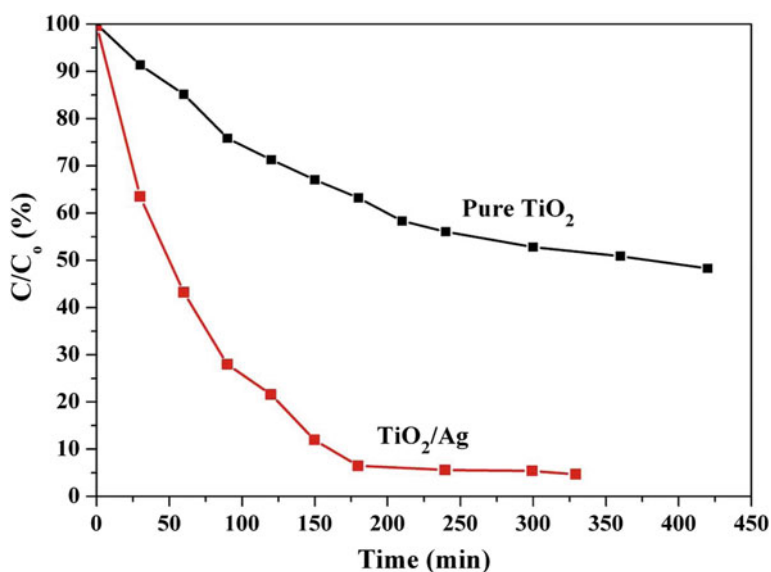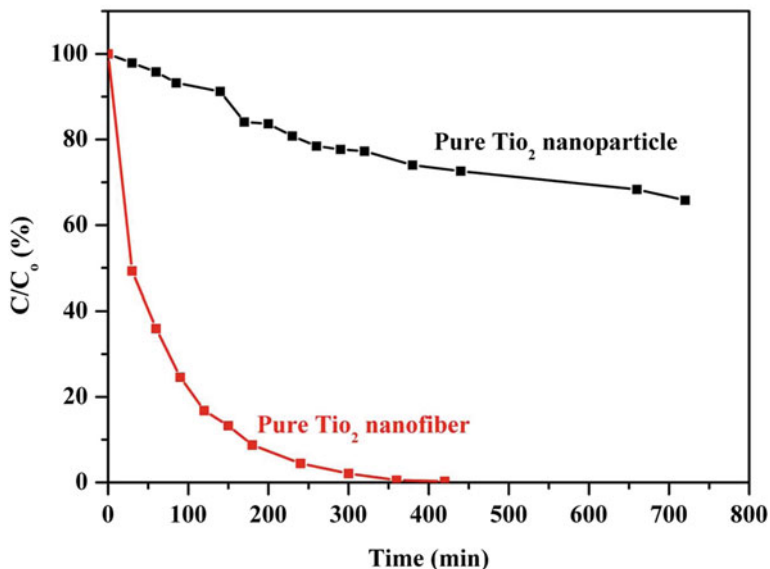

Fig. 10 Photocatalytic degradation of methyl red dye in presence of pure TiO_2 and Ag-TiO_2 nanofibers

photocatalytic activity of pure titanium oxide. As shown in this figure, the nano-fibrous morphology does have great effect. Titanium oxide nanoparticles could not catalyze the photocatalytic reaction to remove the dye even after almost 12 h, 65 % of the original dye was remaining in the solution after such long reaction time. However, the high surface area to volume ration which is the mean feature of nanofibers was the mean reason to get such interesting result compared with nanoparticles. As shown in Fig. 6, all the dye was oxidized and eliminated within 6 h.

Theoretically, some studies have explained the role of silver in enhancing the photocatalytic activity of titania. Generally, these studies have drawn this conclusion: The Ag nanoparticles deposited on TiO_2 surface act as electron acceptors, enhancing the charge separation of electrons and holes and consequently the transfer of the trapped electron to the adsorbed O_2 acting as an electron acceptor. The sufficient dye molecules are adsorbed on the surface of Ag-TiO_2 than on the TiO_2 surface, increasing the photoexcited electron transfer from the sensitized dye molecule to the conduction band of TiO_2 and consequently increasing the electron transfer to the adsorbed O_2.

Experimentally, the silver-doped titania nanofibers and nanoparticles have been invoked as photocatalyst in degradation of methylene blue dye, Fig. 12 shows the obtained results. As shown in this figure, incorporating of silver in titanium oxide nanofibers reveals to significant increase in the degradation rate of this dye. As can be observed in this figure, within 10 min more than 92 % of the dye has been

Fig. 11 Photocatalytic degradation of methylene blue dye in presence of pure TiO_2 nanoparticles
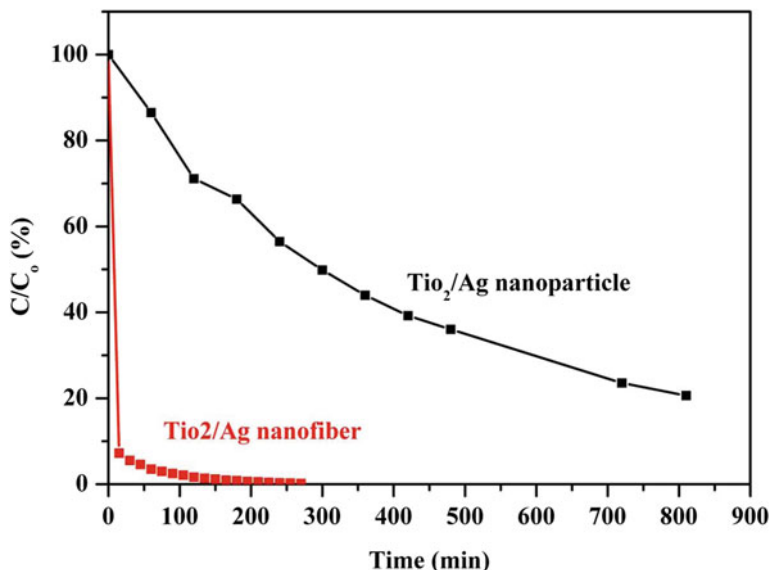
Fig. 12 Photocatalytic degradation of methylene blue dye in presence of Ag-doped TiO_2 nanofibers

degraded, moreover, the dye completely eliminated after almost two hours. This fantastic result comes from exploiting the advantage of the nanofibrous shape as well as the benefit of incorporating of silver in titanium oxide. However, in case of Ag-doped titanium oxide nanoparticles, almost 80 % of the dye has been oxidized after 12 h and the dye did not completely disappeared from the solution.

The results obtained from Figs. 11 and 12 support the pervious works reported the advantages of doping of titanium oxide by silver nanoparticles and simultaneously strongly recommend utilizing this interesting photocatalyst in nanofibrous shape.
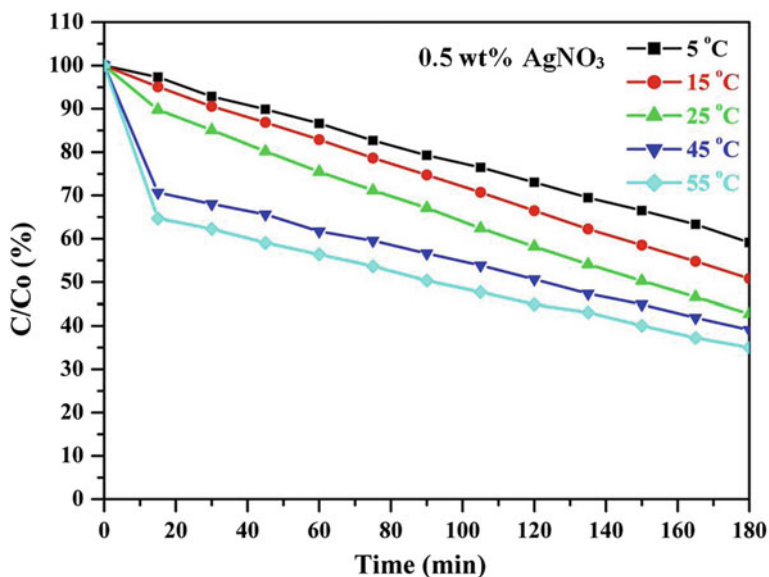
4.4 Effect of Temperature

Photocatalysis is the acceleration of a photoreaction in the presence of a catalyst. In catalyzed photolysis, light is absorbed by an adsorbed substrate. In photogenerated catalysis, the photocatalytic activity depends on the ability of the catalyst to create electron–hole pairs, which generate free radicals (hydroxyl radicals: •OH) able to undergo secondary reactions. Its comprehension has been made possible ever since the discovery of water electrolysis by means of the titanium dioxide.

Figures 13, 14, 15, 16 and 17 represent the photodegrdation of rhodamine B using Ag-doped TiO_2 nanoparticles obtained from sol-gels contain 0.5, 1.0, 1.5, 2.0 and 2.5 wt% $AgNO_3$, respectively at different temperatures (5, 15, 25, 45 and

55 °C). As shown in these figures, increase the silver content in the doped nanoparticles enhances the photoactivity of the utilized photocatalyst. As it is known, increase the reaction temperature improves the photodegretion efficiency. Molecules at a higher temperature have more thermal energy. Although collision frequency is greater at higher temperatures, this alone contributes only a very small proportion to the increase in rate of reaction. Much more important is the fact that the proportion of reactant molecules with sufficient energy to react (energy greater than activation energy: E > Ea) is significantly higher. Accordingly, the dye photodegradation modified linearly with temperature increase. The best temperature was found to be 55 °C, at this temperature the maximum decolorization efficiencies at the utilized reaction time (3 h) were 65, 74, 84, 86 and 100 % for the photocatalyst obtained from sol-gels contain 0.5, 1.0, 1.5, 2.0 and 2.5 wt% $AgNO_3$, respectively. It is noteworthy mentioning that the investigated photocatalyst has good performance only under the UV irradiation as normal light has no impact as shown in Fig. 17.

Table 1 shows the rate of the rhodamine B photodegradation (mg/min) at different temperatures and silver contents. As shown in the table, the maximum rate is not always obtained at the maximum temperature; it depends on the silver content. At the lowest silver content (i.e. 0.5 wt%), the highest rate was obtained at 15 °C. Increasing the silver content shifts the maximum rate to be at 25 °C for the samples obtained from sol-gels having 1.0 and 1.5 wt% silver nitrate. However, at the higher silver contents the best rate was obtained at 45 °C. Overall, the

Fig. 13 Effect of temperature on the degradation rate of rhodamine B dye using Ag-doped TiO_2 nanoparticles having 0.5 wt% $AgNO_3$ under UV irradiation
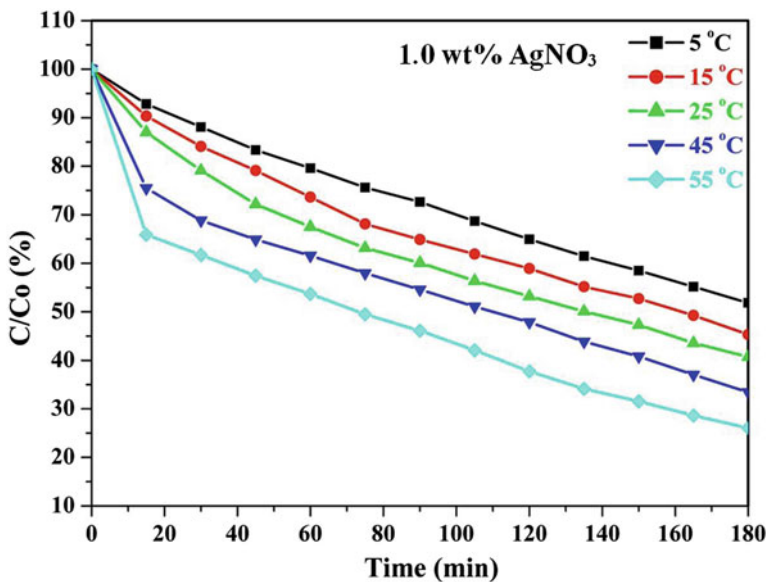
Fig. 14 Effect of temperature on the degradation rate of rhodamine B dye using Ag-doped TiO$_2$ nanoparticles having 1.0 wt% AgNO$_3$ under UV irradiation
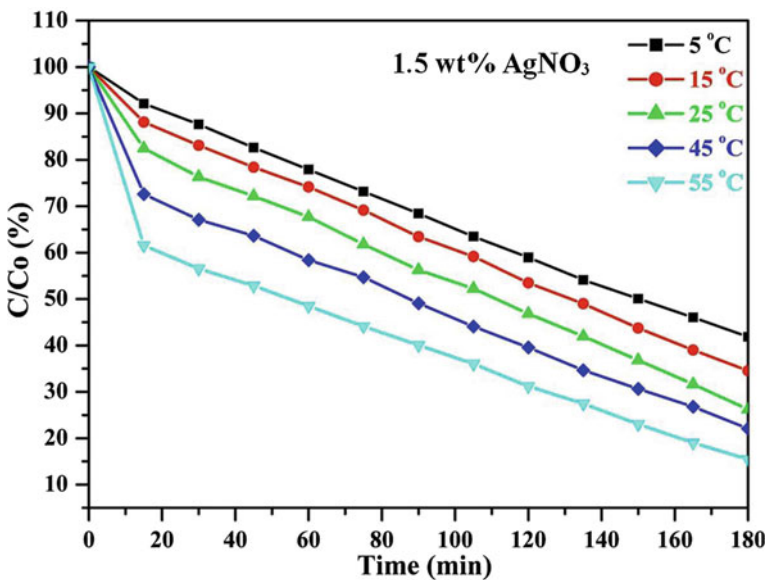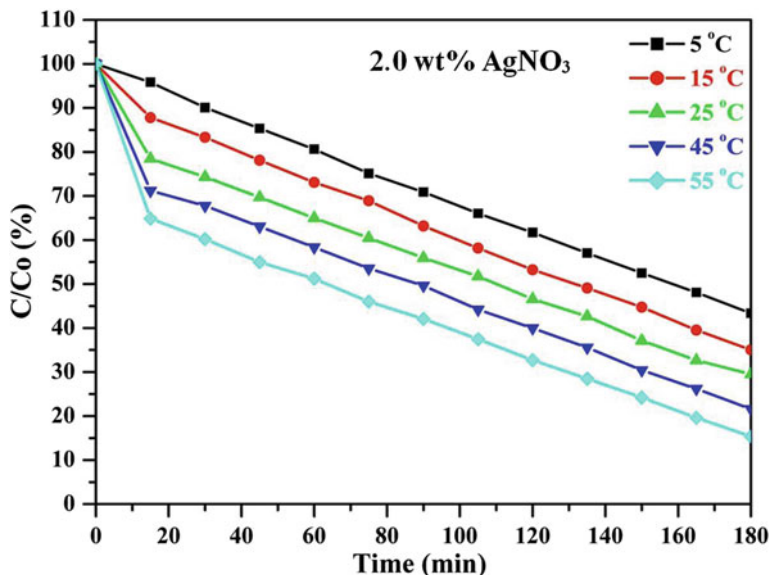

Fig. 15 Effect of temperature on the degradation rate of rhodamine B dye using Ag-doped TiO$_2$ nanoparticles having 1.5 wt% AgNO$_3$ under UV irradiation

Fig. 16 Effect of temperature on the degradation rate of rhodamine B dye using Ag-doped TiO_2 nanoparticles having 2.0 wt% $AgNO_3$ under UV irradiation
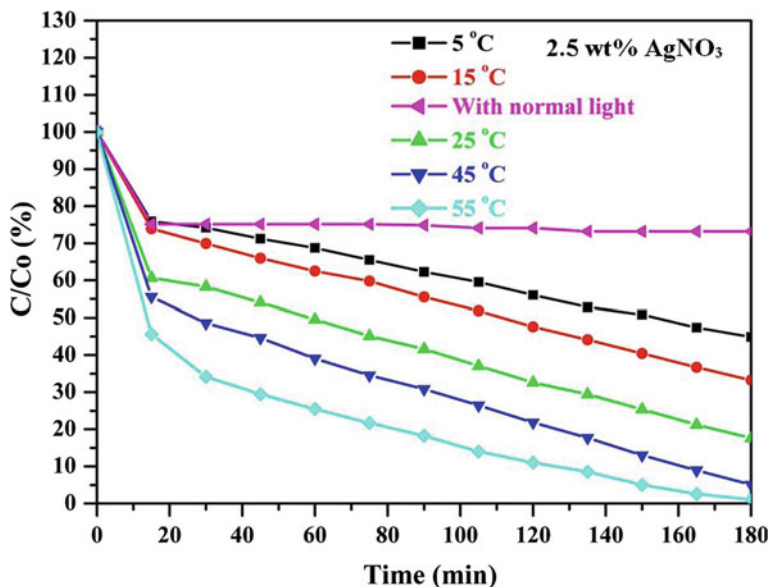

Fig. 17 Effect of temperature on the degradation rate of rhodamine B dye using Ag-doped TiO_2 nanoparticles having 2.5 wt% $AgNO_3$ under UV irradiation, and also at room temperature under the normal light

maximum degradation rate is corresponding to the samples obtained from the sol-gels having 1.0 and 1.5 wt% silver nitrate at the room temperature (0.0356 mg/min). As aforementioned, besides enhancing the activation energy, increase the temperature leads to increase the kinetic energy of the dyes molecules which modifies the collisions with the catalyst surface. If the catalyst surface is very active so numerous free radicals will be present in the thin film surrounding the catalyst nanoparticles, so fast cracking reactions of the dye molecules will take place, otherwise the molecules will escape without degradation. Therefore, for the low silver content NPs, the surface is not so active so relatively low temperature (15 °C) is preferred to provide suitable time for dye molecules to react with the available •OH radicals. Increase the temperature leads to escape the molecules. More increase in the silver content results in more activation of the NPs surfaces, so low contact time is enough to degrade the dye molecules in the thin layer surrounding the catalyst NPs. Accordingly, the maximum degradation rates were obtained at 45 °C for the samples having high silver contents (last two columns in Table 1). At 55 °C, the kinetic energy is high enough to liberate the dye molecules from the active zones before degradation so low degradation rate was obtained. However, the number of the degraded dye molecules is high in the beginning of the reaction (the first 10 min) which makes the quantitative degradation is more at 55 °C. For instance after 10 min, at 55 °C, the eliminated dyes were 35, 38 and 55 % for the nanoparticles obtained from sol-gels containing 0.5, 1.5, and 2.5 wt% silver nitrate, respectively. It is noteworthy to mention that the fast initial degradation in the first 10 min (Figs. 13, 14, 15, 16, 17) made the total elimination of the dyes linearly dependent on the temperature. However, after this initial declination, the photodegrdation rate becomes temperature independent as shown in Table 1.

In contrast to the nanoparticles, influence of temperature was different in case of Ag-doped TiO_2 nanofibers. Figures 18, 19, 20, 21 and 22 represent the photodegrdation of rhodamine B using Ag-doped TiO_2 nanofibers obtained from electrospun nanofiber mats contain 0.5, 1.0, 1.5, 2.0 and 2.5 wt% $AgNO_3$, respectively at different temperatures. As shown in these figures, on contrary to the nanoparticulate morphology, the photodegrdation efficiency was temperature-dependent only at low silver content (0.5 wt%, Fig. 18) as the best degradation was obtained at the highest temperature. Moreover, the amount of the eliminated dyes was

Table 1 Rate of rhodamine B dye removal (mg/min) using Ag-doped TiO_2 nanoparticles

Temperature (°C)	$AgNO_3$ content (wt%)				
	0.5	1.0	1.5	2.0	2.5
5	0.0250	0.0269	0.0313	0.0356	0.0200
15	**0.0313**	0.0288	0.0331	0.0325	0.0269
25	0.0294	**0.0356**	**0.0356**	0.0300	0.0269
45	0.0200	0.0263	0.0325	**0.0319**	**0.0300**
55	0.0181	0.0256	0.0294	0.0306	0.0250
Activation energy	3,625.32	1,885.29	1,989.84	1,800.2	315.337
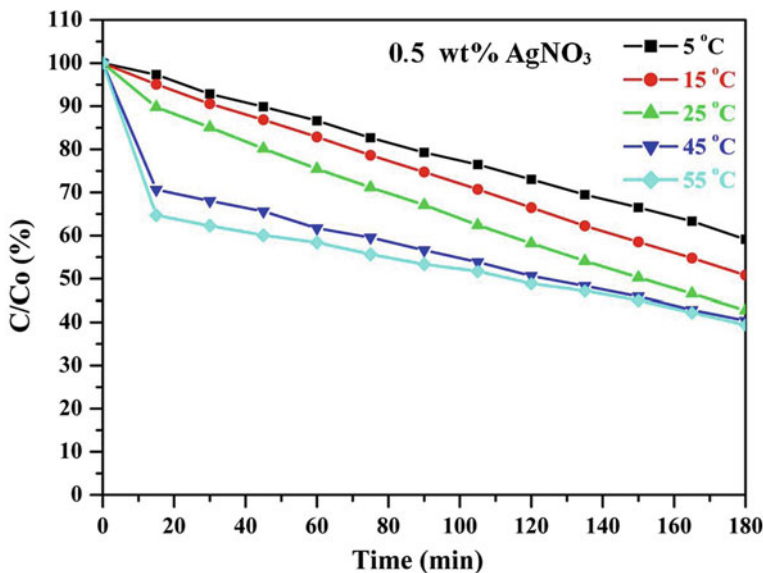
Fig. 18 Effect of temperature on the degradation rate of rhodamine B dye using Ag-doped TiO_2 nanofibers having 0.5 wt% $AgNO_3$ under UV irradiation

gradually and regularly increases with the temperature increase. For the nanofibers obtained from electrospun mats having 1.0 wt% silver nitrate, the optimum reaction temperature was 45 °C as shown in Fig. 19. However, for the remaining formulations the optimum temperature was 25 °C; Figs. 20, 21 and 22. For all formulations, 5 °C reaction temperature is the worst conditions as the lowest degradation was obtained at this temperature. Moreover, contrary to the nanoparticulate morphology, starting from silver nitrate content of 1.0 wt% in the electrospun nanofibers mats, the photodegradation cannot be mathematically correlated with the reaction temperatures as shown in Figs. 19, 20, 21 and 22. These obtained results can be explained by the higher activity of the nanofibrous Ag-doped TiO_2 compared to the nanoparticulate morphology especially at high silver contents. Beside the desorption process and kinetic energy, it is possible also that the temperature affects the e–h pairs transfer and lifetime.

Figure 23 represents a conceptual illustration to explain the influence of the temperature on the photodegradation of the rhodamine B molecules using Ag-doped TiO_2 nanoparticles and nanofibers. In case of nanoparticles, the surface activity is not high so increase the temperature has the normal impact on the chemical reactions and enhances the degradation process in general by modifying the activation energy. However, in case of the nanofibers having high silver content, the surface is very active so instant degradation for the dye molecules takes place at the thin film surrounding the nanofibers. Therefore, increase the temperature which leads to increase the molecules kinetic energy has positive impact in the beginning as it helps to move the molecules to the active zones.
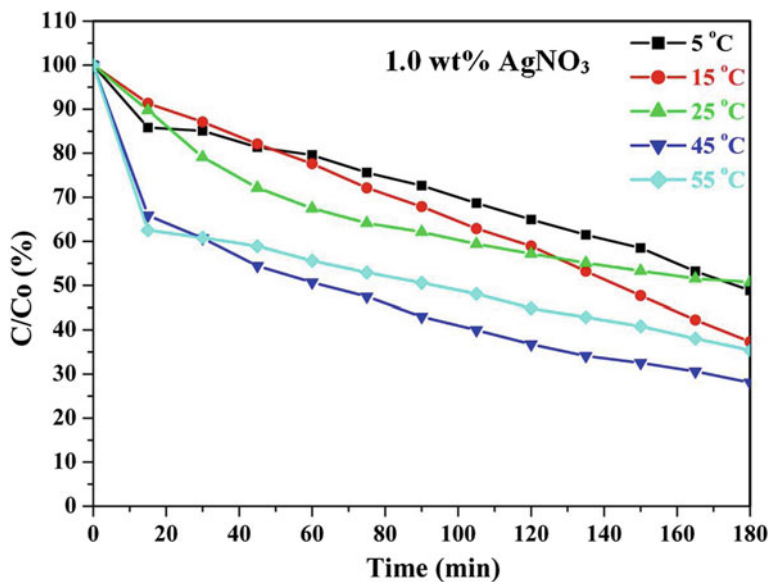
Fig. 19 Effect of temperature on the degradation rate of rhodamine B dye using Ag-doped TiO$_2$ nanofibers having 1.0 wt% AgNO$_3$ under UV irradiation
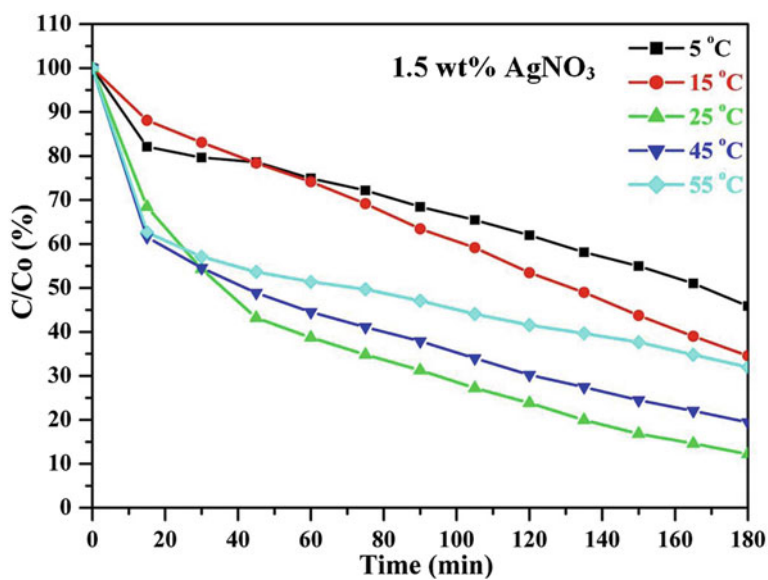

Fig. 20 Effect of temperature on the degradation rate of rhodamine B dye using Ag-doped TiO$_2$ nanofibers having 1.5 wt% AgNO$_3$ under UV irradiation
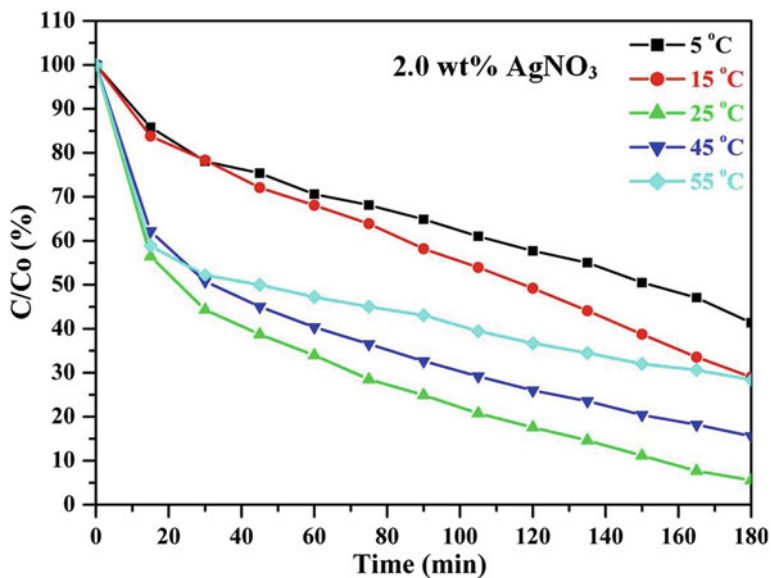
Fig. 21 Effect of temperature on the degradation rate of rhodamine B dye using Ag-doped TiO$_2$ nanofibers having 2.0 wt% AgNO$_3$ under UV irradiation
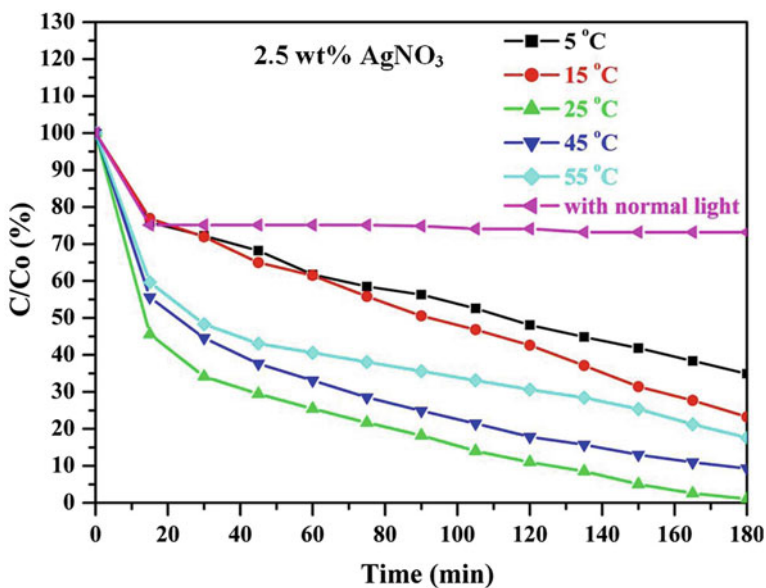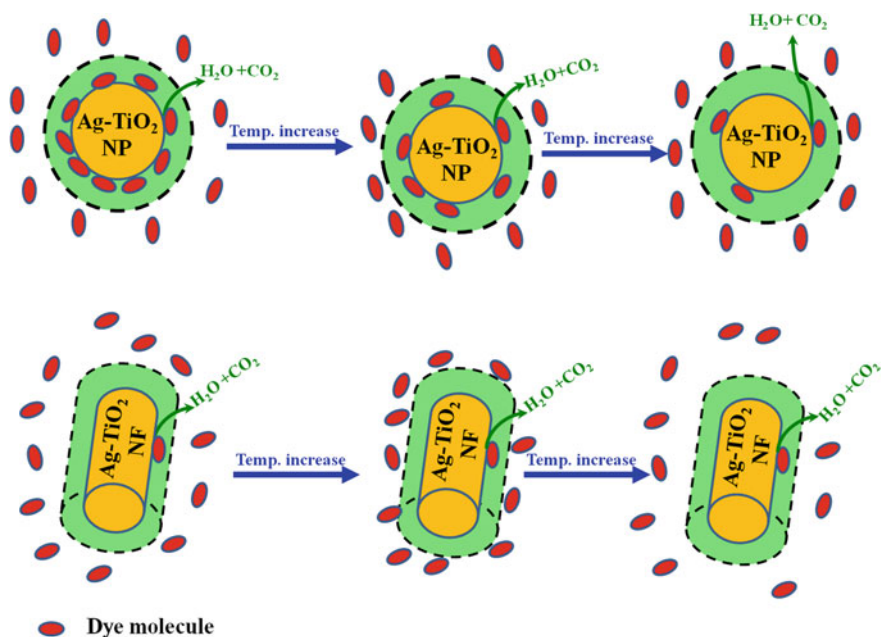

Fig. 22 Effect of temperature on the degradation rate of rhodamine B dye using Ag-doped TiO$_2$ nanofibers having 2.5 wt% AgNO$_3$ under UV irradiation, and also at room temperature under the normal light

However, more increase in the temperature leads to produce kinetic energy able to move away the dye molecules from the active zones before achieving the degradation process. Therefore, for the nanofibers obtained from electrospun mats having silver nitrate more than 1.5 wt% the optimum temperature is 25 °C followed by 45 °C and then 55 °C which means inverse relationship between the photodegradation and the temperature due to increase the kinetic energy of the molecules. In summary, in case of nanofibers, the temperature affects the photodegradation process from the kinetic energy point of view. However, in case of nanoparticles, beside the kinetic energy, temperature can enhance the activation energy which improves the photodegradation process.

Based on the introduced hypothesis; the initial rate should show a positive temperature effect over the nanofibers with high silver content. However, some results (Fig. 13) do not match this expected behavior because the experimental plan was established to detect the first concentration after 10 min. Because the surface is very active, it is believed that if the first samples, in case of nanofibers, were drawn after very short time (e.g. 2 min) the initial rate will be found temperature dependent.

Figure 24 displays the photodegradation of the methylene blue dye using Ag-doped nanoparticles; (A) and nanofibers; (B) at the optimum temperatures (i.e. 55 and 25 °C, respectively). As shown in the figure, the nanofibers have distinct performance compared with the nanoparticles at all silver contents. As shown in

Fig. 23 Schematic diagram illustrates the influence of the temperature on the photodegradation process in case of using the Ag-doped TiO_2 nanoparticles and nanofibers

the figure, 92 % from the dye was degraded in 10 min when Ag-doped TiO_2 nanofibers obtained from electrospun mats containing 2.0 wt% silver nitrate were used as photocatalyst. As aforementioned in the introduction section, silver-doping is a known strategy to enhance the photocatalytic activity of the titanium oxide nanostructure. Therefore, the photocatalytic activity of the both utilized formulations was strongly enhanced upon silver addition as shown in all the obtained results.

The results obtained in Fig. 24 supports the aforementioned hypothesis about the strong activity of the nanofibers surfaces compared to the nanoparticles. Therefore, for the same silver content, distinct difference in the photodegradation performance was obtained as shown in all results. A proposed explanation for this finding can be as follow: as the photodegradation process mainly bases on electrons transfer through the photocatalyst so the structure providing high surface to volume ratio is expected to have better performance because it supplies good electron mobility. Mathematically, it is known that the particulate shape (sphere) has the lowest surface to volume ratio. Therefore, the nanofibrous shape provides more space for the electrons which reflects higher activity compared to the nanoparticles.

4.5 Influence of Silver Doping on the TiO_2 Crystal Structure

Titanium oxide has three popular crystal structures; anatase, rutile and brookite. Anatase is a polymorph with the two other minerals. The minerals rutile and brookite as well as anatase all have the same chemical formula, TiO_2, but they have different structures. Rutile is the more common and the more well known mineral of the three, while anatase is the rarest. Anatase shares many of the same or nearly the same properties as rutile such as luster, hardness and density. However, due to structural differences, anatase and rutile differ slightly in the crystal habit. The phase change from anatase polymorph of titania to rutile one has been the subject of considerable interest and the focus of many groups' activities over the years. Figure 1 shows the effect of silver-doping on the crystal structure of the obtained powder after the calcination process. In case of silver-free solution, the results affirm formation of pure anatase titanium dioxide, existence of strong diffraction peaks at 2θ values of 25.09°, 37.65°, 38.44°, 47.89°, 53.89°, 55.07°, 62.40°, 68.70°, 70.04° and 75.00° corresponding to the crystal planes of (101), (004), (112), (200), (105), (211), (204), (220), (220) and (215), respectively indicates formation of anatase titanium dioxide [JCPDS card no 21-1272]. Addition of small amount of silver nitrate (2 wt%) did not affect the crystal structure of the titania, however pure silver metal was formed due to decomposition of the silver nitrate upon heating. The extra peaks at 2θ values of 38.11°, 44.29°, 64.43° and 77.48°, corresponding to the crystal planes of (111), (200), (220) and (311), respectively affirm presence of silver metal [JCPDS card no 04-0783]. In Fig. 25, the main peaks of anatase and silver were marked as A and S, respectively.
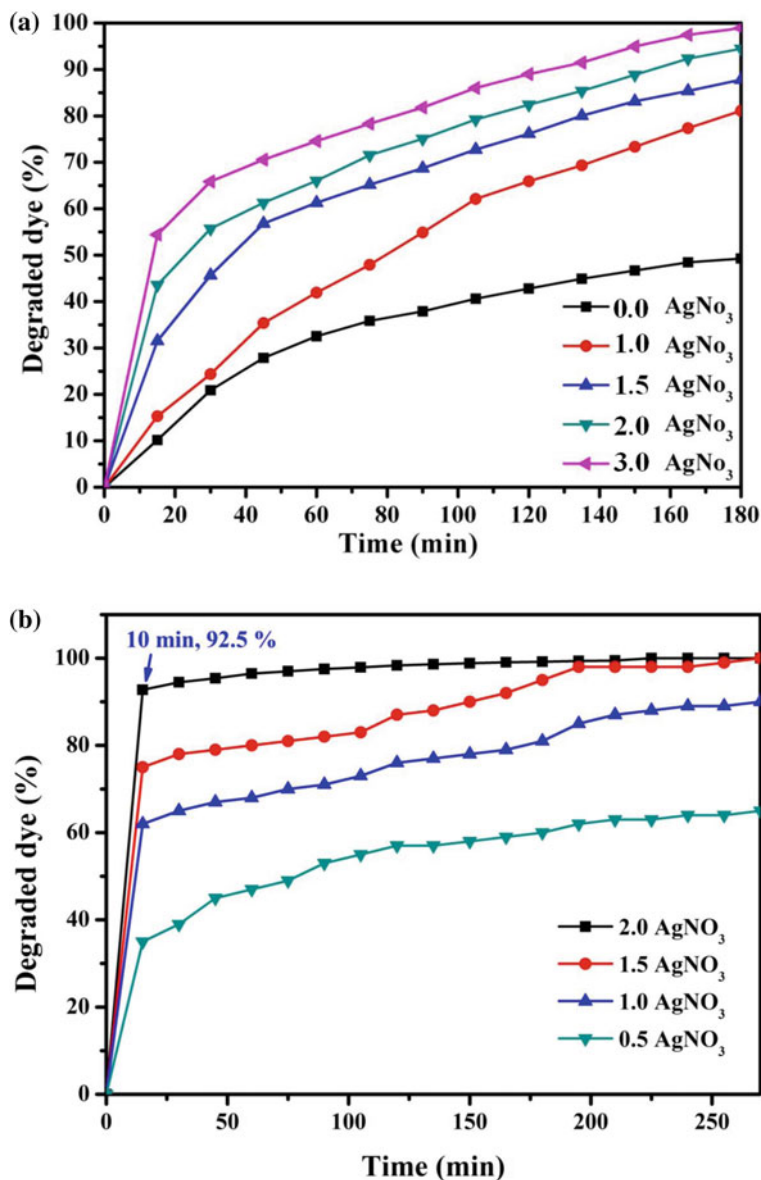
Fig. 24 Photodegradation of methylene blue dye using different Ag-doped TiO_2 in nanoparticulate; a and nanofibrous; b at 55 and 25 °C, respectively

Increase the silver nitrate content to 3 wt% in the original electrospun solution led to partial phase change in the titania crystal structure. The standard peaks of rutile can be observed at 2θ values of 27.45°, 36.09°, 41.23°, 54.32°, 56.64°, and 69.08° corresponding to the crystal planes of (110), (101), (111), (211), (220), and (301),

respectively [JCPDS card no 21-1272]. Interestingly, the results indicate that increase the amount of silver enhances formation rutile phase as shown in Fig. 1 (the main rutile peaks were marked by R letter). Addition of 5 wt% silver nitrate led to increase the rutile content to be higher than the anatase. According to the XRD data, the ratio of rutile to anatase is ∼75 and 440 % when the added silver nitrate was 3 and 5 wt%, respectively.

4.6 Influence of Silver Doping on the Morphology

The electrospinning technique involves the use of a high voltage to charge the surface of a polymer solution droplet and thus to induce the ejection of a liquid jet through a spinneret. Due to bending instability, the jet is subsequently stretched by many times to form continuous, ultrathin fibers. It is widely used for production of many polymeric nanofibers. Moreover, the electrospinning process has been exploited to produce metal oxides nanofibers by calcination of electrospun mats obtained from completely miscible sol–gel solutions. Electrospinning of a sol–gel composed of Ti(IsO) and PVAc/DMF solution has been carried out in our lab in
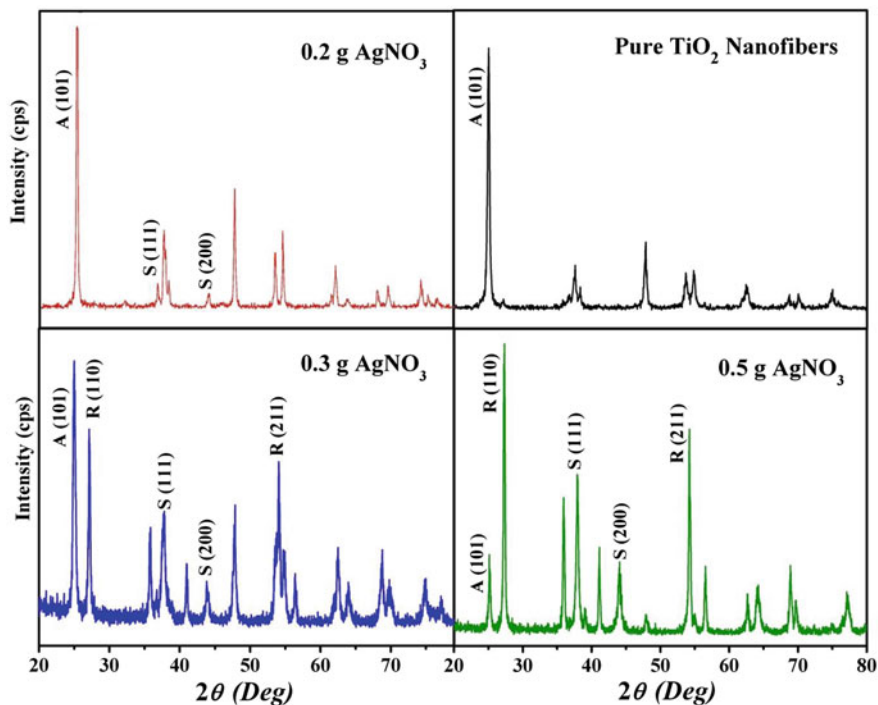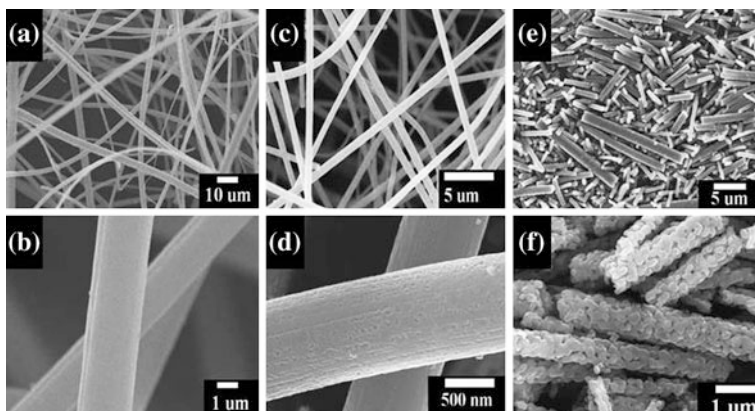

Fig. 25 Effect of silver content on the crystal structure of TiO_2

Fig. 26 Effect of silver content on the nanofibrous morphology of TiO_2

previous study [62], the resultant electrospun nanofibers have good morphology. Addition of silver nitrate to the sol–gel does not affect the morphology [5]. Accordingly, well morphology electrospun nanofibers mats were obtained from $AgNO_3$/Ti(Iso)/PVAc solutions at all the utilized $AgNO_3$ contents (data are not shown). Figure 26 shows the morphology of the resultant powder after the calcination process. As can be observed in Fig. 26a and b which demonstrate the obtained product from silver-free electrospun solution, well and smooth TiO_2 nanofibers were obtained, these nanofibers composed of pure anatase as could be concluded from the XRD results (Fig. 25). Incorporation of small amount of silver does not have considerable impact on the nanofibrous morphology as shown in Fig. 26c and d which represent the FE-SEM images of the powder obtained from calcination of an electrospun solution containing 2 wt% $AgNO_3$. However, the surface became little rough (Fig. 26d).

5 Conclusion

Ag-doped TiO_2 nanofibers can be prepared by calcination of electrospun nanofiber mats obtained from electrospinning of titanium isopropoxide, silver nitrate and poly(vinyl acetate) sol-gels. Also, drying, grinding and calcination of the same sol-gels lead to produce Ag-doped TiO_2 nanoparticles. The obtained nanostructure is having both of antase and rutile phases if the silver nitrate content is more than 3 wt%. Rutile phase content can be increased by increasing the silver content in the original electrospun solution. However, the nanofibrous morphology is strongly affected by the silver-content, excess silver causes to destroy the 1D structure. Silver-doping of the titanium oxide nanofibers greatly enhances the photocatalytic activity of this interesting material. The temperature has positive

impact on the photodegradation when the photocatalyst is exploited in the form of nanoparticles due to modification of the kinetic and the activation energies. However, in case of the nanofibrous morphology, the temperature has negative impact due to the super activity of the surface compared to the nanoparticles. Increase the temperature leads to enhance the kinetic energy of the dyes molecules which leads to escape the molecules from the active zones surrounding the nanofibers. Overall, this study strongly recommends utilizing using the photocatalyst in the form of nanofibers at room temperature as the maximum degradation can be obtained at these conditions.

References

1. Karunakaran, C., Abiramasundari, G., Gomathisankar, P., Manikandan, G., Anandi, V.: Cu-doped TiO2 nanoparticles for photocatalytic disinfection of bacteria under visible light. J. Colloid Interface Sci. **352**, 68–74 (2010)
2. Ou, H.-H., Lo, S.-L.: Effect of Pt/Pd-doped TiO2 on the photocatalytic degradation of trichloroethylene. J. Mol. Catal. A: Chem. **275**, 200–205 (2007)
3. Vorontsov, A., Stoyanova, I., Kozlov, D., Simagina, V., Savinov, E.: Kinetics of the photocatalytic oxidation of gaseous acetone over platinized titanium dioxide. J. Catal. **189**, 360–369 (2000)
4. Li, F., Li, X.: The enhancement of photodegradation efficiency using Pt-TiO2 catalyst. Chemosphere **48**, 1103–1111 (2002)
5. Kanjwal, M.A., Barakat, N.A.M., Sheikh, F.A., Khil, M.S., Kim, H.Y.: Functionalization of electrospun titanium oxide nanofibers with silver nanoparticles: strongly effective photocatalyst. Int. J. Appl. Ceram. Technol. **7**, E54–E63 (2010)
6. Li, X., Li, F.: Study of $Au/Au^{3+}-TiO_2$ photocatalysts toward visible photooxidation for water and wastewater treatment. Environ. Sci. Technol. **35**, 2381–2387 (2001)
7. Tian, Y., Tatsuma, T.: Mechanisms and applications of plasmon-induced charge separation at TiO_2 films loaded with gold nanoparticles. JACS **127**, 7632–7637 (2005)
8. Haynes, C.L., Van Duyne, R.P.: Plasmon-sampled surface-enhanced Raman excitation spectroscopy. J. Phys. Chem. B **107**, 7426–7433 (2003)
9. Hodak, J.H., Martini, I., Hartland, G.V.: Spectroscopy and dynamics of nanometer-sized noble metal particles. J. Phys. Chem. B **102**, 6958–6967 (1998)
10. Zhao, G., Kozuka, H., Yoko, T.: Sol—gel preparation and photoelectrochemical properties of TiO_2 films containing Au and Ag metal particles. Thin Solid Films **277**, 147–154 (1996)
11. Sung-Suh, H.M., Choi, J.R., Hah, H.J., Koo, S.M., Bae, Y.C.: Comparison of Ag deposition effects on the photocatalytic activity of nanoparticulate TiO_2 under visible and UV light irradiation. J. Photochem. Photobiol., A **163**, 37–44 (2004)
12. Wu, T., Liu, G., Zhao, J., Hidaka, H., Serpone, N.: Photoassisted degradation of dye pollutants. V. Self-photosensitized oxidative transformation of rhodamine B under visible light irradiation in aqueous TiO_2 dispersions. J. Phys. Chem. B **102**, 5845–5851 (1998)

13. Sobana, N., Muruganadham, M., Swaminathan, M.: Nano-Ag particles doped TiO$_2$ for efficient photodegradation of Direct azo dyes. J. Mol. Catal. A: Chem. **258**, 124–132 (2006)
14. Arabatzis, I., Stergiopoulos, T., Bernard, M., Labou, D., Neophytides, S., Falaras, P.: Silver-modified titanium dioxide thin films for efficient photodegradation of methyl orange. Appl. Catal., B **42**, 187–201 (2003)
15. Herrmann, J.M., Tahiri, H., Ait-Ichou, Y., Lassaletta, G., Gonzalez-Elipe, A., Fernandez, A.: Characterization and photocatalytic activity in aqueous medium of TiO$_2$ and Ag-TiO$_2$ coatings on quartz. Appl. Catal., B **13**, 219–228 (1997)
16. Damm, C., Israel, G.: Photoelectric properties and photocatalytic activity of silver-coated titanium dioxides. Dyes Pigm. **75**, 612–618 (2007)
17. Shie, J.L., Lee, C.H., Chiou, C.S., Chang, C.T., Chang, C.C., Chang, C.Y.: Photodegradation kinetics of formaldehyde using light sources of UVA, UVC and UVLED in the presence of composed silver titanium oxide photocatalyst. J. Hazard. Mater. **155**, 164–172 (2008)
18. He, X., Zhao, X., Liu, B.: The synthesis and kinetic growth of anisotropic silver particles loaded on TiO$_2$ surface by photoelectrochemical reduction method. Appl. Surf. Sci. **254**, 1705–1709 (2008)
19. Barakat, N.A.M., Abadir, M.F., Nam, K.T., Hamza, A.M., Al-Deyab, S.S., Al-Deyab, S.S., Baek, W.-i., Kim, H.Y.: Synthesis and film formation of iron-cobalt nanofibers encapsulated in graphite shell: magnetic, electric and optical properties study. J. Mater. Chem. **21**, 10957–10964 (2011)
20. Barakat, N.A.M., Khil, M.S., Sheikh, F.A., Kim, H.Y.: Synthesis and optical properties of two cobalt oxides (CoO and Co$_3$O$_4$) nanofibers produced by electrospinning process. J. Phys. Chem. C **112**, 12225–12233 (2008)
21. Kanjwal, M., Barakat, N., Sheikh, F., Baek, W.-i., Khil, M., Kim, H.: Effects of silver content and morphology on the catalytic activity of silver-grafted titanium oxide nanostructure. Fibers Polym. **11**, 700–709 (2010)
22. Arbiol, J., Cerda, J., Dezanneau, G., Cirera, A., Peiro, F., Cornet, A., Morante, J.: Effects of Nb doping on the TiO$_2$ anatase-to-rutile phase transition. J. Appl. Phys. **92**, 853–861 (2002)
23. Li, X., Wang, H., Wu, H.: Phthalocyanines and their analogs applied in dye-sensitized solar cell. Funct Phthalocyanine Mol. Mater. 229–273 (2010)
24. Hegde, R.R., Dahiya, A., Kamath, M.: Nanofiber nonwovens, June (2005)
25. Chowdhury, M.M.R.: Electro spinning process nano fiber and their application
26. Wu, H., Lin, D., Zhang, R., Pan, W.: Facile synthesis and assembly of Ag/NiO nanofibers with high electrical conductivity. Chem. Mater. **19**, 1895–1897 (2007)
27. Doshi, J., Reneker, D.H.: Electrospinning process and applications of electrospun fibers. J. Electrostat. **35**, 151–160 (1995)
28. Shin, Y., Hohman, M., Brenner, M., Rutledge, G.: Experimental characterization of electrospinning: the electrically forced jet and instabilities. Polymer **42**, 09955–09967 (2001)
29. Han, T., Yarin, A.L., Reneker, D.H.: Viscoelastic electrospun jets: Initial stresses and elongational rheometry. Polymer **49**, 1651–1658 (2008)
30. Xia, Y., Yang, P., Sun, Y., Wu, Y., Mayers, B., Gates, B., Yin, Y., Kim, F., Yan, H.: One-Dimensional Nanostructures: synthesis, characterization, and applications. Adv. Mater. **15**, 353–389 (2003)
31. Law, M., Goldberger, J., Yang, P.: Semiconductor nanowires and nanotubes. Ann. Rev. Mater. Res. **34**, 83–122 (2004)
32. Sun, Y., Khang, D.Y., Hua, F., Hurley, K., Nuzzo, R.G., Rogers, J.A.: Photolithographic route to the fabrication of micro/nanowires of III–V semiconductors. Adv. Funct. Mater. **15**, 30–40 (2004)
33. Li, D., Xia, Y.: Electrospinning of nanofibers: reinventing the wheel? Adv. Mater. **16**, 1151–1170 (2004)
34. Reneker, D.H., Chun, I.: Nanometre diameter fibres of polymer, produced by electrospinning. Nanotechnology **7**, 216 (1999)
35. Chronakis, I.S.: Novel nanocomposites and nanoceramics based on polymer nanofibers using electrospinning process—a review. J. Mater. Process. Technol. **167**, 283–293 (2005)

36. Sheikh, F.A., Barakat, N.A.M., Kanjwal, M.A., Park, S.J., Park, D.K., Kim, H.Y.: Synthesis of poly (vinyl alcohol)(PVA) nanofibers incorporating hydroxyapatite nanoparticles as future implant materials. Macromol. Res. **18**, 59–66 (2010)

37. Kc, R.B., Kim, C.K., Khil, M.S., Kim, H.Y., Kim, I.S.: Synthesis of hydroxyapatite crystals using titanium oxide electrospun nanofibers. Mater. Sci. Eng., C **28**, 70–74 (2008)

38. Aoi, K., Aoi, H., Okada, M.: Synthesis of a poly (vinyl alcohol)-based graft copolymer having poly (ε-caprolactone) side chains by solution polymerization. Macromol. Chem. Phys. **203**, 1018–1028 (2002)

39. Kim, C.H., Khil, M.S., Kim, H.Y., Lee, H.U., Jahng, K.Y.: An improved hydrophilicity via electrospinning for enhanced cell attachment and proliferation. J. Biomed. Mater. Res. B Appl. Biomater. **78**, 283–290 (2006)

40. Tang, Z., Wei, J., Yung, L., Ji, B., Ma, H., Qiu, C., Yoon, K., Wan, F., Fang, D., Hsiao, B.S.: UV-cured poly (vinyl alcohol) ultrafiltration nanofibrous membrane based on electrospun nanofiber scaffolds. J. Membr. Sci. **328**, 1–5 (2009)

41. Chuang, W.Y., Young, T.H., Yao, C.H., Chiu, W.Y.: Properties of the poly (vinyl alcohol)/chitosan blend and its effect on the culture of fibroblast in vitro. Biomaterials **20**, 1479–1487 (1999)

42. Lai, Y., Sun, L., Chen, C., Nie, C., Zuo, J., Lin, C.: Optical and electrical characterization of TiO_2 nanotube arrays on titanium substrate. Appl. Surf. Sci. **252**, 1101–1106 (2005)

43. Lai, Y., Chen, Y., Zhuang, H., Lin, C.: A facile method for synthesis of Ag/TiO_2 nanostructures. Mater. Lett. **62**, 3688–3690 (2008)

44. Xu, M.W., Bao, S.J., Zhang, X.G.: Enhanced photocatalytic activity of magnetic TiO_2 photocatalyst by silver deposition. Mater. Lett. **59**, 2194–2198 (2005)

45. Hufschmidt, D., Bahnemann, D., Testa, J.J., Emilio, C.A., Litter, M.I.: Enhancement of the photocatalytic activity of various TiO_2 materials by platinisation. J. Photochem. Photobiol., A **148**, 223–231 (2002)

46. Nikolajsen, T., Leosson, K., Bozhevolnyi, S.I.: Surface plasmon polariton based modulators and switches operating at telecom wavelengths. Appl. Phys. Lett. **85**, 5833–5835 (2004)

47. Huang, P., Wu, F., Zhu, B., Gao, X., Zhu, H., Yan, T., Huang, W., Wu, S., Song, D.: CeO_2 nanorods and gold nanocrystals supported on CeO_2 nanorods as catalyst. J. Phys. Chem. B **109**, 19169–19174 (2005)

48. Zhang, L., Yu, J.C.: A simple approach to reactivate silver-coated titanium dioxide photocatalyst. Catal. Commun. **6**, 684–687 (2005)

49. Herrmann, J.M., Disdier, J., Pichat, P.: Photoassisted platinum deposition on TiO_2 powder using various platinum complexes. J. Phys. Chem. **90**, 6028–6034 (1986)

50. Mulvaney, P., Giersig, M., Henglein, A.: Electrochemistry of multilayer colloids: preparation and absorption spectrum of gold-coated silver particles. J. Phys. Chem. **97**, 7061–7064 (1993)

51. Herrmann, J.M.: Termodynamic considerations of strong metal-support interaction in a real $PtTiO_2$ catalyst. J. Catal. **118**, 43–52 (1989)

52. Herrmann, J.M., Disdier, J., Pichat, P.: Effect of chromium doping on the electrical and catalytic properties of powder Titania under UV and visible illumination. Chem. Phys. Lett. **108**, 618–622 (1984)

53. Cozzoli, P.D., Comparelli, R., Fanizza, E., Curri, M.L., Agostiano, A., Laub, D.: Photocatalytic synthesis of silver nanoparticles stabilized by TiO_2 nanorods: a semiconductor/metal nanocomposite in homogeneous nonpolar solution. JACS **126**, 3868–3879 (2004)

54. Tian, R., Wang, X., Li, M., Hu, H., Chen, R., Liu, F., Zheng, H., Wan, L.: An efficient route to functionalize singe-walled carbon nanotubes using alcohols. Appl. Surf. Sci. **255**, 3294–3299 (2008)

55. Mai, L., Wang, D., Zhang, S., Xie, Y., Huang, C., Zhang, Z.: Synthesis and bactericidal ability of Ag/TiO_2 composite films deposited on titanium plate. Appl. Surf. Sci. **257**, 974–978 (2010)

56. Marques, H., Canário, A., Moutinho, A., Teodoro, O.: Work function changes in the Ag deposition on TiO_2 (110). Vacuum **82**, 1425–1427 (2008)

57. Barakat, N.A.M., Kanjwal, M.A., Al-Deyab, S.S., Chronakis, I.S., Kim, H.Y.: Influences of silver-doping on the crystal structure, morphology and photocatalytic activity of TiO_2 nanofibers. Mater. Sci. Appl. **2** (2011)
58. Barakat, N.A.M., Kim, B., Park, S.J., Jo, Y., Jung, M.-H., Kim, H.Y.: Cobalt nanofibers encapsulated in a graphite shell by an electrospinning process. J. Mater. Chem. **19**, 7371–7378 (2009)
59. Barakat, N.A.M., Woo, K.-D., Kanjwal, M.A., Choi, K.E., Khil, M.S., Kim, H.Y.: Surface plasmon resonances, optical properties, and electrical conductivity thermal hystersis of silver nanofibers produced by the electrospinning technique. Langmuir **24**, 11982–11987 (2008)
60. Barakat, N.A.M., Hamza, A., Al-Deyab, S.S., Qurashi, A., Kim, H.Y.: Titanium-based polymeric electrospun nanofiber mats as a novel organic semiconductor. Mater. Sci. Eng., B (2011)
61. Barakat, N.A.M., Shaheer Akhtar, M., Yousef, A., El-Newehy, M., Kim, H.Y.: Pd-Co-doped carbon nanofibers with photoactivity as effective counter electrodes for DSSCs. Chem. Eng. J. (2012)
62. Ding, B., Kim, C.K., Kim, H.Y., Seo, M.K., Park, S.J.: Titanium dioxide nanofibers prepared by using electrospinning method. Fibers Polym. **5**, 105–109 (2004)
63. Xiao, Q., Zhang, J., Xiao, C., Tan, X.: Photocatalytic decolorization of methylene blue over $Zn_{1-x}Co_xO$ under visible light irradiation. Mater. Sci. Eng., B **142**, 121–125 (2007)
64. Mascolo, G., Comparelli, R., Curri, M., Lovecchio, G., Lopez, A., Agostiano, A.: Photocatalytic degradation of methyl red by TiO_2: comparison of the efficiency of immobilized nanoparticles versus conventional suspended catalyst. J. Hazard. Mater. **142**, 130–137 (2007)